

The Influences of Boundary Layer Mixing and Cloud-Radiative Forcing on Tropical Cyclone Size

YIZHE PEGGY BU

Department of Atmospheric and Oceanic Sciences, University of California, Los Angeles, Los Angeles, California

ROBERT G. FOVELL AND KRISTEN L. CORBOSIERO

Department of Atmospheric and Environmental Sciences, University at Albany, State University of New York, Albany, New York

(Manuscript received 7 August 2016, in final form 9 January 2017)

ABSTRACT

Tropical cyclone (TC) size is an important factor directly and indirectly influencing track, intensity, and related hazards, such as storm surge. Using a semi-idealized version of the operational Hurricane Weather Research and Forecasting Model (HWRF), the authors show that both enabling cloud-radiative forcing (CRF) and enhancing planetary boundary layer (PBL) vertical mixing can encourage wider storms by enhancing TC outer-core convective activity. While CRF acts primarily above the PBL, eddy mixing moistens the boundary layer from below, both making peripheral convection more likely. Thus, these two processes can cooperate and compete, making their influences difficult to deconvolve and complicating the evaluation of model physics improvements, especially since the sensitivity to both decreases as the environment becomes less favorable. Further study shows not only the magnitude of the eddy mixing coefficient but also the shape of it can determine the TC size and structure.

1. Introduction

Tropical cyclone (TC) size is an important forecast metric as it directly and indirectly influences TC motion, intensity, track, and storm surge (e.g., Fiorino and Elsberry 1989; Fovell and Su 2007; Lin and Chavas 2012; Carrasco et al. 2014). There are a variety of metrics used to define the TC size, including the radius of the outermost closed isobar, the radius of vanishing wind, and the radius of 34-kt (about 17.5 m s^{-1}) wind speed R_{34} . In this study, R_{34} at 10 m above mean sea level (MSL) is used to define the storm size or width.

Bu et al. (2014) demonstrated that cloud-radiative forcing (CRF), the interaction of hydrometeors with longwave and shortwave radiation, has an important role in expanding the storm size. Averaged through a diurnal cycle, CRF consists of pronounced cooling along the anvil top and weak warming through the cloudy air. In particular, the within-cloud warming was relevant, enhancing convective activity in the TC outer core, leading to a wider eye, a broader tangential wind field,

and a stronger secondary circulation. This forcing also functions as a positive feedback (Fovell et al. 2016), assisting in the development of a thicker and more radially extensive anvil than would otherwise have formed. CRF itself depends on the microphysics parameterization and Fovell et al. (2010) showed it is a major reason why simulations can be sensitive to microphysical assumptions.

Bu et al. (2014) also demonstrated that the GFDL-derived radiation scheme that was long employed operationally in the Hurricane Weather Research and Forecasting Model (HWRF) (cf. Tallapragada et al. 2014) did not handle CRF properly, resulting in deep clouds that were effectively transparent. Testing revealed, however, that implementing an ostensibly superior radiation scheme degraded model skill (L. Bernardet et al. 2014, personal communication). Analysis of those results led us to consider how the planetary boundary layer (PBL) influences storm size, in cooperation and competition with CRF, which is the subject of this study.

It is widely appreciated that boundary layer processes play an important role in TCs (e.g., Smith 1968; Ooyama 1969; Emanuel 1986; Van Sang et al. 2008). Among these processes are mixing acting on momentum and scalars

Corresponding author e-mail: Prof. Robert Fovell, rfovell@albany.edu

such as temperature and moisture, the subgrid portion of which can be represented via diffusion coefficients K_m and K_h , respectively. Models such as HWRP typically handle vertical mixing within the PBL via a parameterization that presumes a local or nonlocal closure (cf. Stensrud 2007; Kepert 2012) such as the Mellor–Yamada–Janjić (MYJ; Janjić 1990) and Yonsei University (YSU; Hong et al. 2006; Hong 2010) schemes, respectively; Nolan et al. (2009a) provide a succinct comparison of these two approaches. Eddy mixing in local schemes depends on the specification of a vertical mixing length l_v , stability, and either the vertical wind shear or prognosed turbulent kinetic energy. HWRP (Tallapragada et al. 2014, 2015) has been using a nonlocal scheme called Global Forecast System (GFS) that, like YSU, is based on Troen and Mahrt (1986) and evolved from the Medium-Range Forecast Model (MRF)’s PBL parameterization (Hong and Pan 1996).

There have been many papers addressing the sensitivity of simulated TCs to PBL parameterizations and assumptions (e.g., Braun and Tao 2000; Hill and Lackmann 2009; Nolan et al. 2009a,b; Smith and Thomsen 2010; Kepert 2012). Most previous studies of the PBL–TC relationship have focused on TC intensity, inner-core convection, and/or the TC PBL structure. A few studies, however, have explicitly examined the influence of the vertical diffusion on the storm structure, most of them reporting no significant influence. For example, Bryan (2012) found the 34-kt-wind radius to be only weakly sensitive (and the radius of maximum wind, or RMW, to be insensitive) to l_v , at least when reasonable values of the horizontal mixing length l_h and the enthalpy–drag coefficient ratio ($C_k/C_d = 0.5$) are used. Bryan and Rotunno (2009) and Chavas and Emanuel (2014) both demonstrated that the RMW remained essentially unchanged with doubled l_v . While Frisius (2015) did find some sensitivity to vertical diffusion, he pointed out that the lifetime of real TCs is too short for the effect of vertical diffusion to become relevant.

With HWRP, we demonstrate herein that vertical mixing can exert a very important influence on storm size within several days after initialization, especially when the operational GFS PBL scheme is employed. In that scheme, the PBL depth h is determined using an iterative bulk Richardson approach calculated from the surface upward. The profile of vertical eddy diffusivity applied to momentum between the surface and h is obtained via

$$K_m = \kappa(U_* / \phi_m)Z[\alpha(1 - Z/h)^2], \quad (1)$$

where κ is the von Kármán constant ($=0.4$), U_* is the surface friction velocity scale, ϕ_m is the wind profile

function (nondimensional shear) evaluated at the top of the surface layer, and Z is the height above the surface. This formula produces a mixing coefficient profile that is parabolic in shape between the surface and h with a maximum at $Z = h/3$. The vertical eddy diffusivity for temperature and moisture K_h is obtained by dividing K_m by the turbulent Prandtl number (Pr ; Hong and Pan 1996). For the GFS scheme as implemented in HWRP, $Pr \approx 1$ within the hurricane PBL, making K_h approximately equal to K_m , but the handling of this proportionality differs even among closely related schemes such as YSU (Hong and Pan 1996; Hong et al. 2006; Hong 2010).¹

Gopalakrishnan et al. (2013) demonstrated that eddy mixing strongly influences the intensity and depth of the TC low-level inflow and the GFS PBL parameterization was producing excessively large K_m values relative to those estimated from observations by Zhang et al. (2011a). They addressed this shortcoming of the GFS scheme by incorporating a tuning parameter α into (1). While a value of $\alpha = 0.25$ was found to produce the most reasonable results relative to the observations at 500 m MSL for wind speeds in the range of 10–60 ms^{-1} , a setting of $\alpha = 0.7$ was adopted in the 2013 and 2014 operational versions of HWRP (Bernardet et al. 2013; Holt et al. 2014) in all three of its telescoping domains as a consequence of skill testing against retrospective TC cases. However, this may have introduced a mismatch between the PBL and surface schemes when $\alpha \neq 1$ that, while addressed in the 2016 operational version of HWRP (W. Wang 2016, personal communication), persists in the version employed herein. The influence of α on the near-surface wind and vertical shear and its consequences are explored in section 3b(3).

In this study, we focus on uncovering how and why the PBL vertical mixing impacts horizontal TC structure and size. The model and experimental design are discussed in section 2. Section 3 demonstrates how and why CRF and PBL mixing cooperate, and compete, to influence TC size. Section 4 presents the summary discussion.

2. Model and experimental design

The HWRP simulations in this study were carried out using the 2014 operational code. These experiments are “semi-idealized” in that we simplified the operational configuration by excluding land and decoupling the

¹ Additionally, according to the WRF code, version 3.7.1, YSU applies a separate mixing coefficient K_q to moisture, which in the mixed layer utilizes a somewhat modified turbulent Prandtl number formulation from that employed for K_h . This results in slightly different mixing being applied to moisture and heat.

ocean model, employing a uniform and constant sea surface temperature (SST) of 302.5 K for the standard runs, and initializing with a horizontally homogeneous tropical sounding [modified from Jordan (1958); see Fovell et al. (2010)] without any mean flow. The Cao et al. (2011) “bubble” procedure was used to initiate the TC and all simulations spanned 4 full days with composite model fields being constructed for the final day in a vortex-following fashion, averaging over one full diurnal cycle. While changes in operational settings (primarily with respect to horizontal smoothing) from the 2013 version used by Bu et al. (2014) resulted in somewhat weaker storms for the same experimental design, all of the standard SST HWRP TCs attained major hurricane status (at least category 3 on the Saffir–Simpson scale) for the analysis period. Please note that most figures employ azimuthal averaging, thereby understating the maximum intensity of these asymmetric, beta-sheared storms (cf. Bender 1997; Bu et al. 2014).

As in Bu et al. (2014), our simulations employed three telescoping domains (with 27-, 9-, and 3-km horizontal grid spacings) along with some of the model physics used operationally during the 2014 season, such as the simplified Arakawa–Schubert (SAS) cumulus parameterization (remaining active in the 27- and 9-km domains after 24 h). In 2014, the operational configuration (cf. Tallapragada et al. 2014) also included the GFDL radiation scheme, the GFS PBL, and the tropical Ferrier microphysics parameterization (MP). These are compared to (or replaced by) RRTMG radiation (Iacono et al. 2008), the YSU PBL (Hong 2010), and Thompson MP (Thompson et al. 2008), respectively. Bu et al. (2014) showed that while RRTMG and GFDL generate nearly identical clear-sky radiative forcing profiles owing to longwave and shortwave radiation (see their Fig. 7a), CRF was not properly handled in the HWRP implementation of the latter. Therefore, owing to their strong similarity with RRTMG cases in which cloud-radiative forcing is deactivated (cf. Bu et al. 2014), HWRP simulations with GFDL radiation are also labeled “CRF-off” herein. Our work has shown that storm structure is significantly modulated by microphysical assumptions (cf. Fovell et al. 2016), but for simplicity we will focus solely on the Thompson scheme.

Also following Bu et al. (2014) we employ an axisymmetric version of Cloud Model 1 (CM1) (Bryan and Rotunno 2009) initialized with the Rotunno and Emanuel (1987) sounding. These simulations used 3-km radial grid spacing and 100-m resolution in the vertical (below 4 km MSL), were initialized with a weak vortex, and were integrated for 12 full days. As in Bu et al. (2014), Goddard radiation (Chou and Suarez 1994) and a version of Thompson microphysics were used for

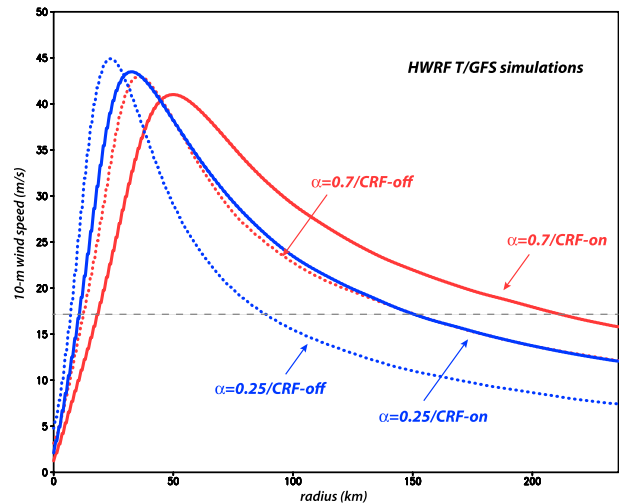


FIG. 1. Radial profiles of temporally and azimuthally averaged 10-m wind speed from semi-idealized HWRP simulations using the GFS PBL and Thompson (“T”) MP varying the α parameter (0.7 in red, 0.25 in blue) and cloud-radiative forcing (CRF-on solid, CRF-off dashed). The CRF-on and CRF-off simulations utilized RRTMG and GFDL radiation, respectively; see text. Gray dashed line indicates 34-kt (17.5 m s^{-1}) speed threshold R_{34} .

most experiments and the latitude was 20°N . Unless otherwise noted, the SST was 299 K as in Bryan and Rotunno (2009), the lower SST being motivated by this sounding’s cooler surface air temperature [see also Bryan (2012)]. All CM1 fields shown are averaged between days 10 and 12, inclusive, except in section 3d, in which an 8–12-day averaging interval was adopted for consistency with Bryan and Rotunno (2009).

3. Results

a. PBL cooperation with CRF

As reviewed above, Bu et al. (2014) demonstrated that CRF plays an important role in determining TC structure. This can be seen in HWRP simulations made using Thompson (“T”) microphysics and the GFS PBL scheme with either RRTMG (labeled CRF-on) or GFDL radiation (labeled CRF-off) for $\alpha = 0.7$ and 0.25 in (1), representing the 2014 operational model setting and the recommendation of Gopalakrishnan et al. (2013), respectively. Enabling CRF can increase the storm size (as manifested by the 10-m R_{34}) by a substantial (and MP-dependent) amount (cf. solid and dashed red, or solid and dashed blue contours in Fig. 1) because hydrometers interact with radiation to force gentle ascent, elevating the relative humidity through a deep layer mainly above the PBL, resulting in enhanced convective activity in the TC outer core. Although some details (including magnitude) are dependent on microphysics, resolution, and other

factors, the expected pattern of net cooling along cloud top with warming through much of the cloudy area is seen in the T/RRTMG simulation (Fig. 2a), but not in its T/GFDL counterpart (Fig. 2b). The anvil cloud in the case with effective CRF is thicker and also wider, in part because cloud-radiative forcing itself acts as a positive feedback on anvil extent, as demonstrated in Fovell et al. (2016, see their Fig. 11.20).

After we identified the GFDL scheme's lack of cloud-radiative forcing for deep clouds, the Developmental Testbed Center (DTC) and the HWRP team evaluated the RRTMG scheme along with the Thompson MP for adoption in the operational HWRP (see introduction). Their analyses of retrospective simulations demonstrated that the HWRP forecast skill was generally degraded when the new physics was included and, as a consequence, neither package was adopted for the 2014 TC season. The T/RRTMG model storms developed a positive size bias, which was especially pronounced among the Atlantic cases. In the east Pacific subset, the T/RRTMG cases tended to exhibit positive biases early on, but encountered colder SSTs sooner, resulting in negative size biases at longer forecast lead times.

Our working hypothesis was that excessive mixing associated with the GFS scheme with $\alpha \approx 1$, including the value selected for the operational model, compensated for the model's tendency to produce overly small TCs, which was actually a consequence of the missing CRF. Therefore, when the radiation problem was fixed, the model was left with a positive size bias. Put another way, we believe that an improved implementation of CRF justifies a smaller value of vertical eddy diffusivity, at least in the context of the GFS PBL scheme.²

Consistent with this interpretation, Fig. 1 reveals that CRF and α have qualitatively similar influences on horizontal storm size. Note that varying α (for fixed CRF) causes the 34-kt-wind radius to increase significantly independent of the radiation scheme employed (cf. red and blue contour pairs). For instance, with GFDL radiation, increasing α from 0.25 (blue dashed) to 0.7 (red dashed) shifts R_{34} from 90 to 150 km. The narrowest storm used the $\alpha = 0.25$ value suggested by Gopalakrishnan et al. (2013) with GFDL radiation, while the widest employed the 2014/15 operational setting (0.7) with RRTMG. Thus, it is seen that the physics interplay between CRF and mixing can alter the 34-kt-wind radius by factor of 2, and there is a material impact on the eye size as well.

² It is noted that for the 2015 HWRP (Tallapragada et al. 2015), the α parameter was replaced by a strategy that does not require an externally set free parameter. See Bu and Fovell (2015) for more information.

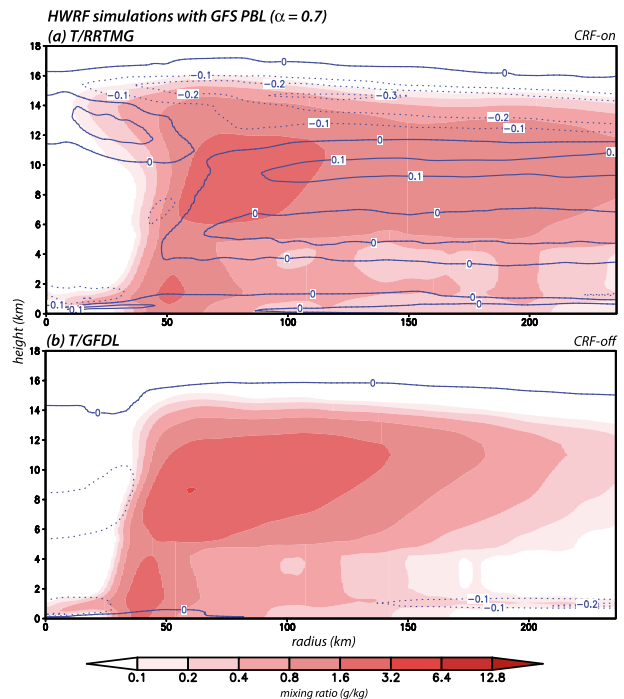


FIG. 2. Temporally and azimuthally averaged total condensation (shaded, note logarithmic scale) and net radiation [negative (dashed) and positive (solid), contour interval 0.1 K h^{-1}] for Thompson/GFS storms using $\alpha = 0.7$ with (a) RRTMG (labeled CRF-on) and (b) GFDL (labeled CRF-off) radiation.

We note that the range of R_{34} found in the experiments above (e.g., 90–205 km) is consistent with observations of TC size derived from ships, buoys, aircraft reconnaissance, and satellite-derived algorithms [see review in Knaff et al. (2016)]. These include an interquartile range of 138–277 km in the Atlantic basin extended best-track (Kimball and Mulekar 2004), 1.8° -mean (1° standard deviation) satellite-derived 34-kt radius of Wu et al. (2015) in the western North Pacific TCs, and range of 90–300 km in Atlantic basin storms with concurrent Hurricane Wind Analysis System (H*Wind) and QuikSCAT data (Chavas et al. 2015).

b. Vertical eddy mixing influence on storm size

1) SENSITIVITY TO α

The expansion of the 34-kt-wind radius seen in Fig. 1 occurs because the PBL mixing acts in a very similar manner as CRF in expanding storm size, as illustrated by the temporally and spatially averaged microphysical diabatic tendency and tangential wind fields shown in Fig. 3. Implementing CRF for fixed α (right column) and varying α with CRF active (left column) both result in a radially more extended heating field, causing the wind field (as illustrated by the tangential wind differences in

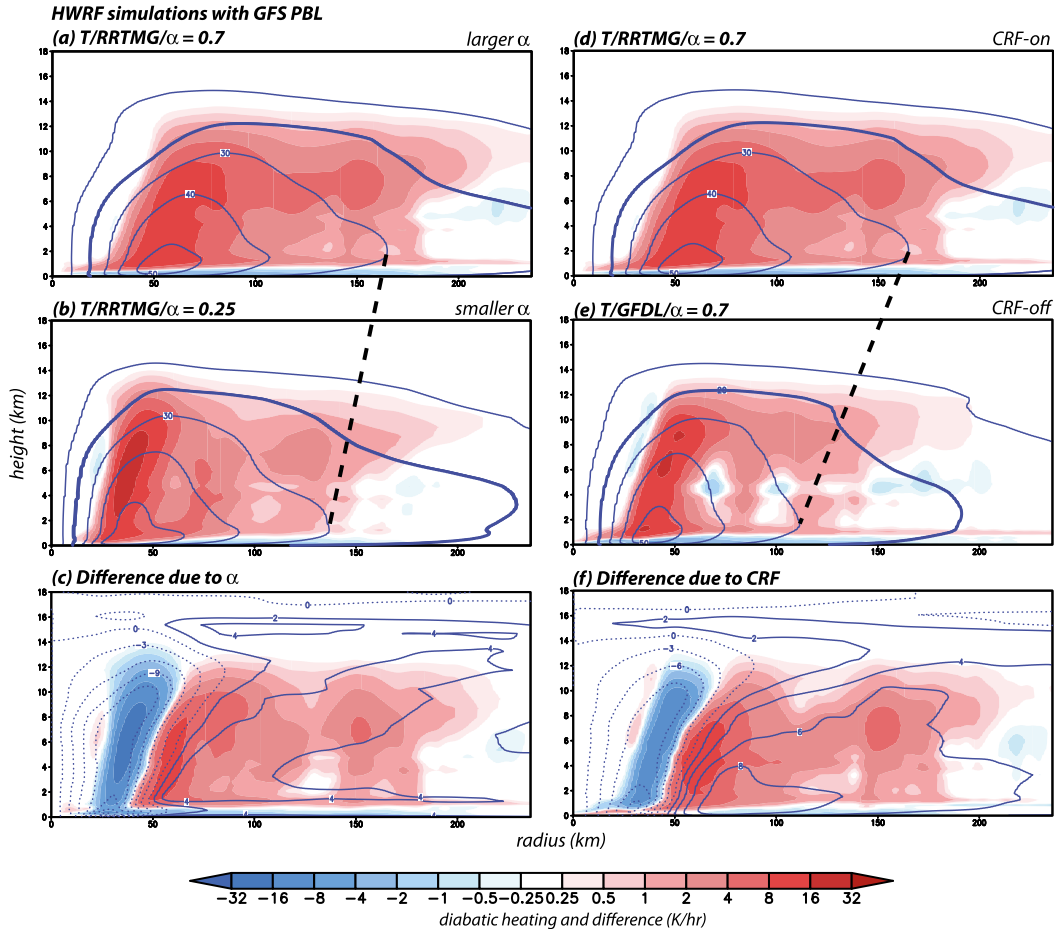


FIG. 3. Radius vs height cross sections showing the temporally averaged symmetric components of microphysics diabatic forcing (shaded) and tangential wind (10 m s^{-1} contours) from Thompson/RRTMG simulations using the GFS PBL with (a) $\alpha = 0.7$ and (b) $\alpha = 0.25$. (c) The $\alpha = 0.7$ minus $\alpha = 0.25$ difference fields; the superposed field is tangential velocity difference (1 m s^{-1} contours). Also shown are Thompson/GFS simulations with $\alpha = 0.7$ for the (d) RRTMG radiation and (e) GFDL radiation cases. (f) The RRTMG minus GFDL difference fields. To facilitate comparisons, (a) and (d) are identical.

the bottom row) to expand outward in qualitatively similar manners, for the reasons discussed in Bu et al. (2014). The impact on the eye size is also obvious in the difference plots. Note that while the GFDL/ $\alpha = 0.7$ and RRTMG/ $\alpha = 0.25$ runs possessed nearly identical 10-m-wind profiles (Fig. 1), their tangential winds differed more substantially aloft. We are focusing on the 10-m winds because these are used in skill assessments. However, these results serve as a reminder that the near-surface winds alone may not be sufficient to accurately determine actual storm size.

As noted above, the α parameter was added to (1) to control eddy mixing in the TC inner core with the GFS PBL scheme. Figure 4a shows vertical profiles of K_m from T/RRTMG/GFS simulations, averaged over an annulus residing between 30 and 200 km from the center for various α values, with the corresponding

near-surface-wind profiles presented in Fig. 5a. The profiles differ little with respect to vertical shape, which is determined by (1) and the PBL depth h . However, increasing α causes R_{34} to increase monotonically from 150 to more than 250 km and for the RMW to shift outward as well. These profiles represent very different storm sizes but essentially the same fundamental structures when nondimensionalized with respect to maximum wind speed (V_{max}) and RMW (Fig. 5b). The modified Rankine slope parameter between one and four multiples of the RMW is about 0.65, very near the upper bound determined by Mallen et al. (2005) for all TCs ranging from prehurricane to major hurricane intensity.

One important and direct impact of the eddy mixing is associated with the vertical transport of water vapor in the boundary layer, upward from the sea surface to the PBL top. Figures 6a–c, which present water vapor and

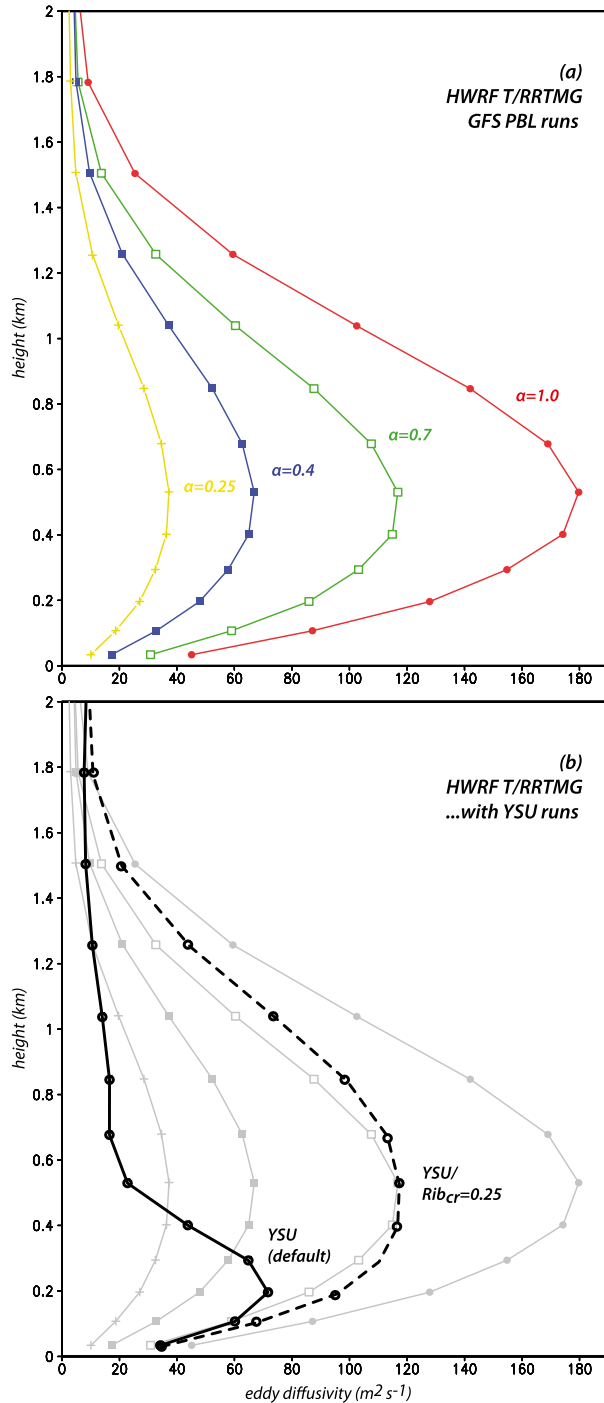


FIG. 4. Profiles of vertical eddy diffusivity ($\text{m}^2 \text{s}^{-1}$) averaged in time and through an annulus extending from 30 to 200 km from the storm center, for T/RRTMG simulations. (a) Momentum and scalar diffusivity ($K_m = K_h$) from runs with $\alpha = 1.0, 0.7, 0.4,$ and 0.25 . (b) As in (a), but showing scalar eddy diffusivity K_h from YSU simulations using the default and modified Rib_{cr} values superimposed.

K_h fields for T/RRTMG storms with $\alpha = 0.7$ and 0.25 along with their differences, demonstrate that the more substantial mixing produced with larger α is associated with higher moisture content in the upper portion of the PBL, especially at larger radii. This pattern is consistent with the contribution of vertical eddy mixing to the local water vapor (q_v) tendency, which is a second-order parabolic term of the form

$$\left[\frac{\partial q_v}{\partial t} \right]_{\text{mix}} = \frac{\partial}{\partial z} \left(K_h \frac{\partial q_v}{\partial z} \right). \quad (2)$$

In the atmosphere, the water vapor concentration decreases quasi linearly with height and, as a consequence of the parabolic vertical shape of K_h , we would expect negative vapor tendencies where K_h increases with height (below the level where K_h reaches its maximum) and positive tendencies where K_h decreases with height (above the K_h maximum). This also applies to the difference fields, and explains the positive values above, and negative ones below, the level of maximum K_h difference (Fig. 6c). Thus, one contributor leading to the greater PBL moisture (≥ 400 m above the sea surface) in the larger α run is enhanced vertical mixing. The enhanced water vapor transport to the top of the PBL brings the air there closer to saturation, which can encourage more convective activity, producing the diabatic heating that eventually leads to a broader wind field [see discussion in Bu et al. (2014) and Fovell et al. (2016)].

Figures 6d–f extend the comparison to two simulations varying CRF for fixed α and illustrate two important points. First, CRF *itself* induces a change in the PBL mixing. This is not surprising as the parameterized mixing responds to the circulation changes induced by cloud–radiation interaction. Second, the effect of altered mixing on the vapor field in this experiment is dominated by the CRF influence, which is sizable and not confined to the boundary layer. As a consequence, we will explicitly control the PBL mixing in some subsequent sensitivity tests in order to separate these two effects.

2) INFLUENCE OF SST ON α SENSITIVITY

Examination of DTC's HWRFT retrospective cases from their initial Thompson and RRTMG tests described above suggested to us that the impact of α could vary from case to case, and even from region to region, with some TCs being quite insensitive to the value employed. From these cases, we surmised that the less convectively favorable the environment, the less influence eddy mixing of moisture would, or could, have. Within the

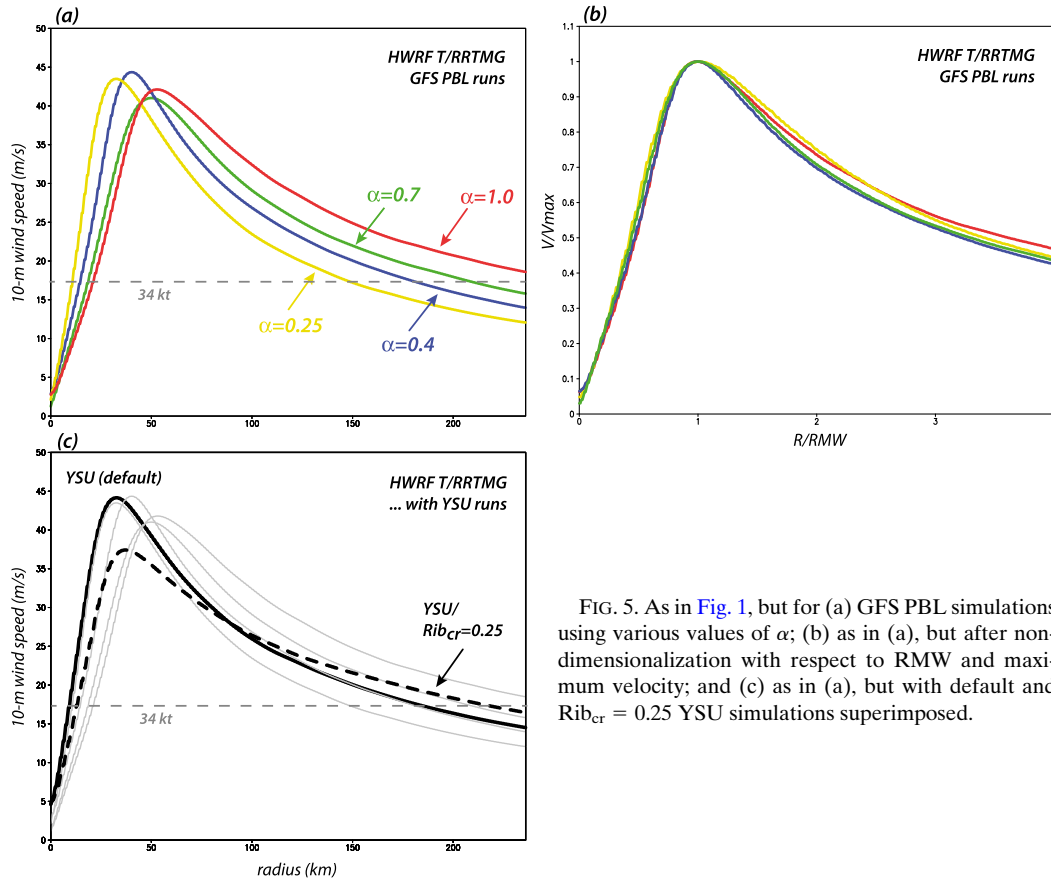


FIG. 5. As in Fig. 1, but for (a) GFS PBL simulations using various values of α ; (b) as in (a), but after non-dimensionalization with respect to RMW and maximum velocity; and (c) as in (a), but with default and $Rib_{cr} = 0.25$ YSU simulations superimposed.

semi-idealized framework, we can establish a more unfavorable environment by simply lowering the SST from its standard value of 302.5 K. In this subsection, we explore how SST modulates the impact of α on the storm size, selecting values of 300 and 298 K to examine.

Colder SSTs result in smaller and weaker storms, other factors being equal (Fig. 7), consistent with Holland (1997), Lin et al. (2015), and Chavas et al. (2016), and the disparity between the larger and smaller α diminishes as well. While the water vapor and K_h difference fields for these cooler-SST cases (Fig. 8) resemble those of the standard case (Fig. 6c), the magnitudes are markedly smaller. Less vapor is being transported upward through the PBL and, as a consequence, outer-core convective activity and winds are correspondingly weaker. Thus, the storms are more compact.

In this experiment, there are two convolved factors: the diminished entropy supply from the sea surface directly reduces the storm intensity but also indirectly decreases the eddy mixing since K_m (and K_h) is proportional to U_* , which itself depends on the near-surface wind speed. These factors can be separated

in a straightforward way with an axisymmetric version of CM1, which uses a version of Thompson microphysics and a radiation scheme (Goddard) that is comparable to RRTMG. In this special assessment, CM1’s vertical mixing is deactivated and replaced with azimuthally and temporally averaged K_m and K_h fields derived from the HWRF’s control run with $\alpha = 1$ that, although not explicitly shown, closely resembles that in Fig. 6a but with larger magnitude (see also Fig. 4). We set $K_m = K_h$ so $Pr = 1$ as is typical in the GFS scheme. These fields are imposed from the initial time and held fixed, making them independent of the model physics and dynamics, and their magnitudes easy to manipulate.

Figure 9 shows temporally averaged 10-m-wind profiles for four different SSTs for these “fixed K ” simulations using both the original and decreased amounts of mixing. For the latter, K_m and K_h are still equivalent but reduced by a factor of 3. It is worth noting that these CM1 storms tend to be stronger (in terms of maximum 10-m wind) than their HWRF counterparts, in part because they cannot develop asymmetries. However, it is clear that as the SST is lowered, the storms become both smaller and less sensitive to the magnitude of the eddy mixing, the

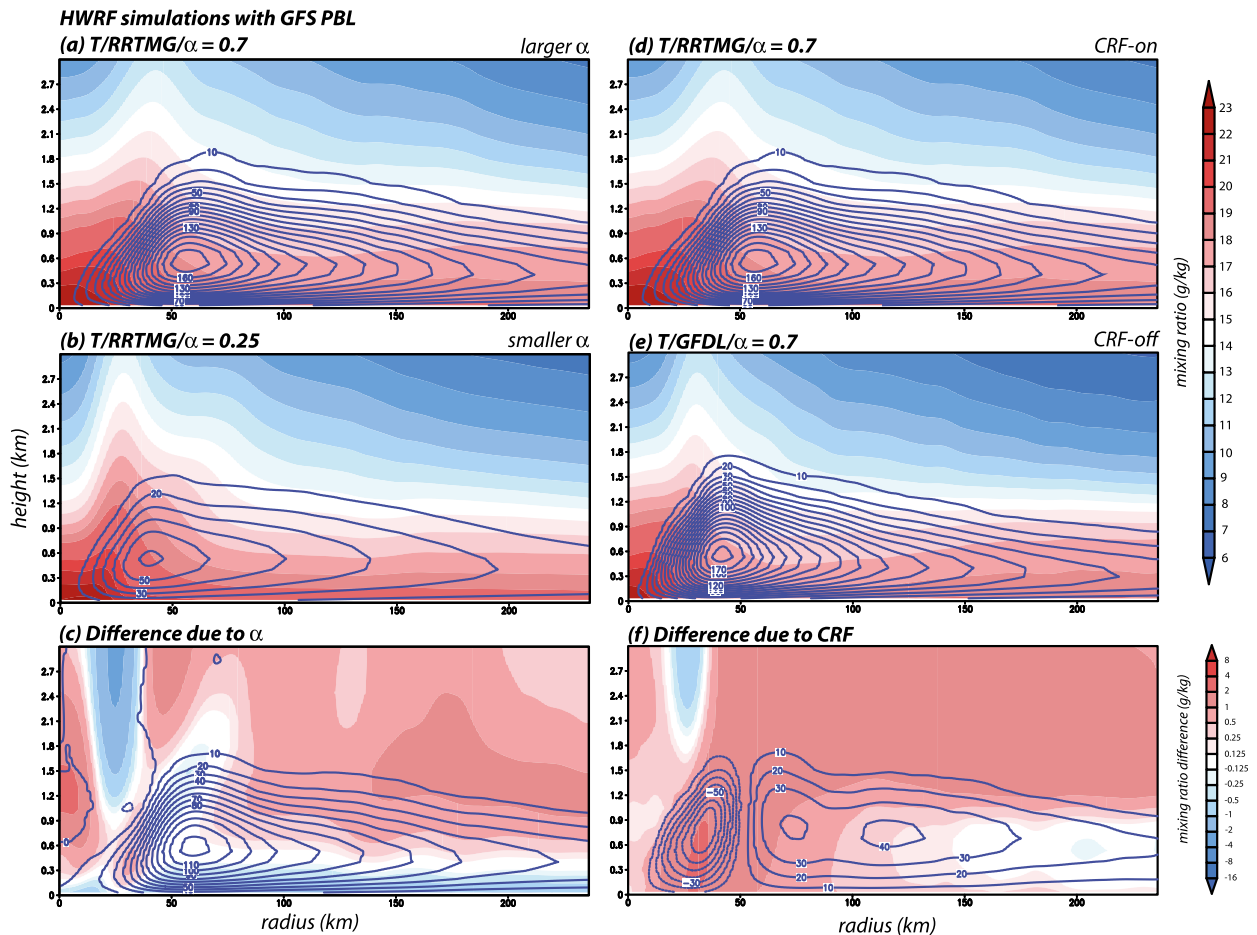


FIG. 6. Similar to Fig. 3, but showing water vapor (shaded) and eddy diffusivity applied to vapor K_h ($10 \text{ m}^2 \text{ s}^{-1}$ contours), for HWRf Thompson simulations using the GFS PBL. (a) $\alpha = 0.7$, (b) $\alpha = 0.25$, and (c) difference fields. (d) CRF-on, (e) CRF-off, and (f) difference fields. Note that, to facilitate comparisons, (a) and (d) are identical.

radial size differences being 42%, 31%, and 21% for SSTs of 299, 297, and 295 K, respectively. Less favorable environments contain less available vapor and thus mixing has a diminished influence on storm structure.

Thus, it appears that TC size can be directly modulated via water vapor transport in the boundary layer, with the sensitivity to α values gradually disappearing as the entropy supply from the sea surface declines. This reveals that the inclusion of lower-sensitivity cases could serve to partially obscure the influence of PBL mixing in ensemble statistics incorporating a large number of events.

We note in passing that in both the HWRf and CM1 mixing experiments (Figs. 7 and 9), the intensity difference between greater and lesser mixing is not a simple function of SST. TC intensity is a complex function of many factors, including available energy from the sea surface as well as the competition between inner- and outer-core convective activity (e.g., May and Holland

1999; Wang 2009; DeMaria et al. 2012). Although decreasing the water vapor diffusion through the whole domain may suppress the convection in the eyewall region somewhat, the outer convection may be reduced even more. As a consequence, the net influence may be to actually intensify the TC; this deserves further study.

3) INFLUENCE OF α ON SCALARS AND MOMENTUM

We have shown that the unmodified GFS PBL parameterization produces vigorous mixing and reducing this via α results in the model storms becoming smaller. Since $K_h = K_m \text{Pr}^{-1}$ and the scheme yields $\text{Pr} \approx 1$ in the hurricane boundary layer, this means that manipulating α modifies the momentum and scalar mixing equally. We now examine HWRf simulations in which K_m or K_h are reduced separately, without explicitly modifying the other mixing coefficient, using the $\alpha = 1$ simulation included in Fig. 5a as the control run. This can be

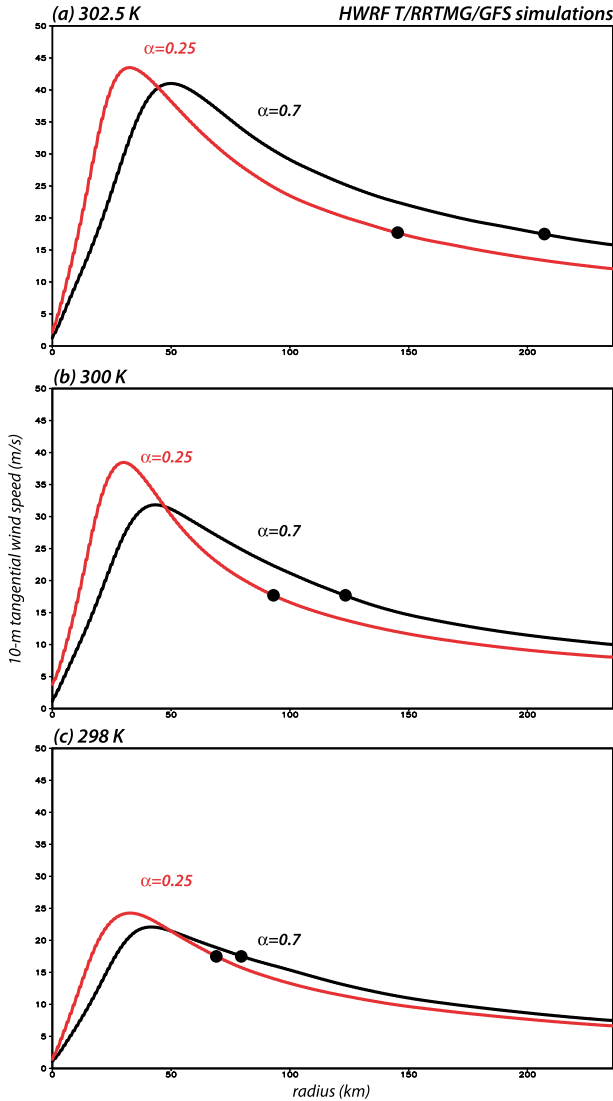


FIG. 7. As in Fig. 1, but for T/RRTMG/GFS simulations with $\alpha = 0.7$ (black) and $\alpha = 0.25$ (red) for SSTs of (a) 302.5, (b) 300, and (c) 298 K. Black dots indicate 34-kt-wind radii.

considered a selective application of α and/or a direct manipulation of Pr, the handling of which varies among parameterizations. As an example, the YSU scheme, the subject of the next subsection, develops $Pr < 1$ in the hurricane PBL, meaning relatively larger diffusion is applied to scalars than to momentum.

The experiment reveals that the mixing applied to scalars (being water vapor, temperature, and non-precipitating condensate for GFS) has a greater influence on storm size than that applied to momentum. Reducing the mixing applied to these fields by two-thirds (without explicitly modifying K_m) results in a substantially narrower storm than in the control run, not only at the 10-m level (Fig. 10a) but also through an

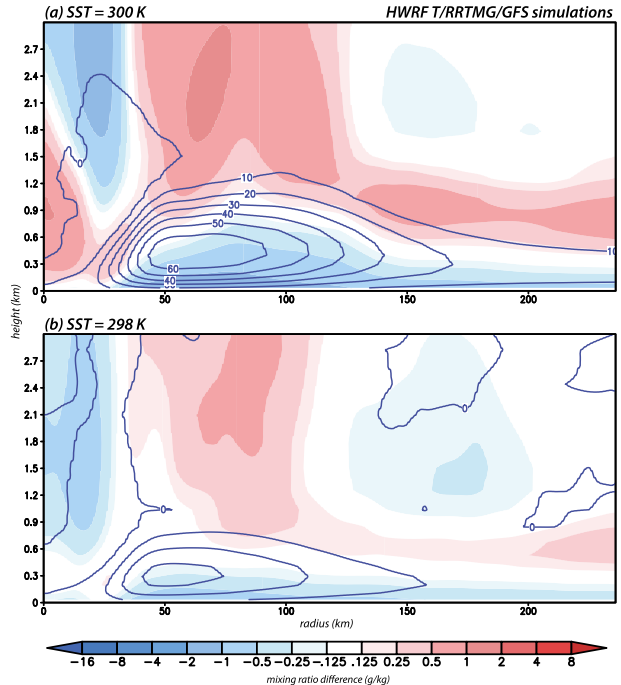


FIG. 8. As in Fig. 6c, but showing vapor and K_h difference fields between $\alpha = 0.7$ and $\alpha = 0.25$ simulations with SSTs of (a) 300 and (b) 298 K.

appreciably deep layer, as revealed by vertical profiles of wind speed averaged through the 100–250-km annulus (Fig. 10b) and vertical cross sections of tangential wind and diabatic heating (Figs. 11a,b). Consistent with our prior findings, the diabatic heating fields suggest the narrowness is a consequence of diminished convective activity beyond the TC inner core. Furthermore, this result is mainly driven by vapor diffusion, as reducing the mixing applied to water vapor alone suffices to accomplish most of the storm contraction [simulation labeled $K_h/3$ (vapor only)].

In contrast, manipulating the momentum vertical diffusion (without explicitly modifying K_h) has a much smaller overall impact on storm width. In this example, the effect appears large (and comparable to scalar mixing reduction) at the 10-m level (Figs. 10a,b), but what has changed most is the near-surface vertical shear as the wind profile farther aloft is less affected (Figs. 10b and 11c). This result may be anticipated with a version of (2) acting on the horizontal wind speed U :

$$\left[\frac{\partial U}{\partial t} \right]_{\text{mix}} = \frac{\partial K_m}{\partial z} \frac{\partial U}{\partial z} + K_m \frac{\partial^2 U}{\partial z^2}. \quad (3)$$

The first term on the right-hand side dominates because the wind profile just above the surface lacks curvature. The value of K_m increases with height to $Z \approx 0.5$ km

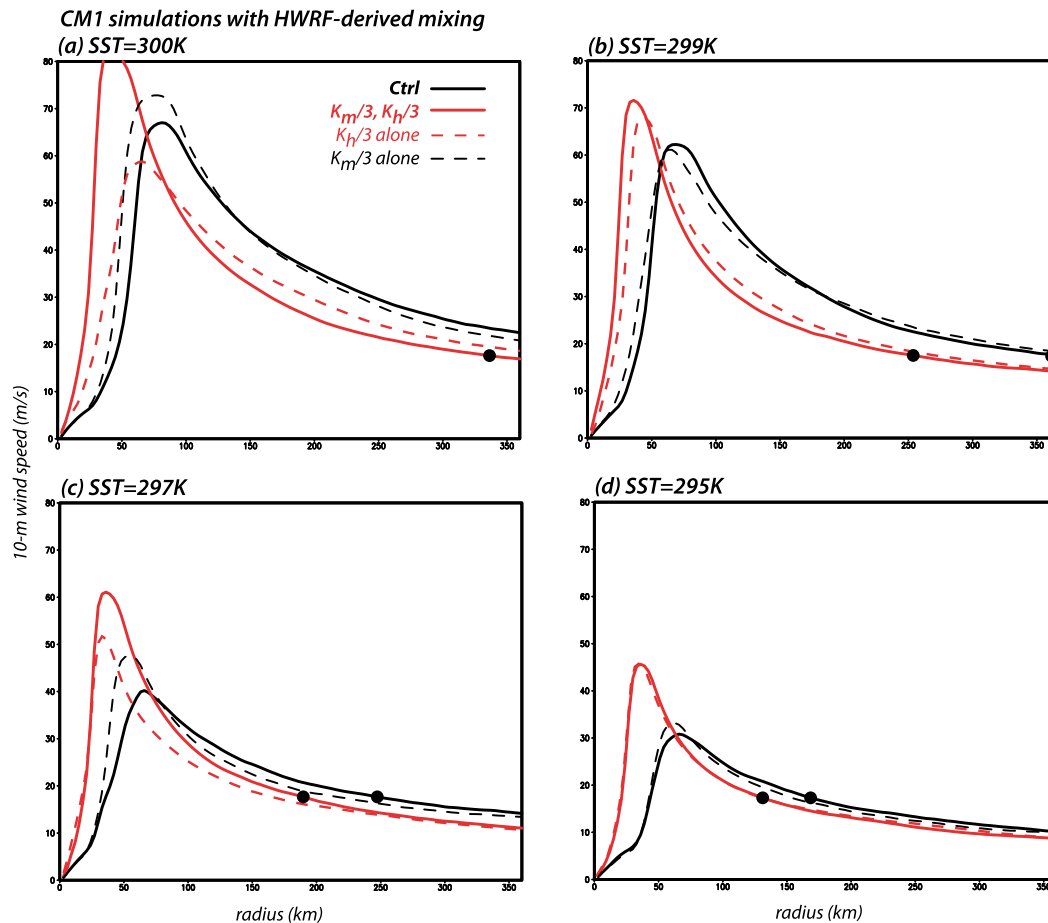


FIG. 9. The 10-m wind speeds (m s^{-1}) vs radius averaged between days 8 and 12 for “fixed K ” CM1 axisymmetric simulations imposed with K_m and K_h profiles from HWRf’s $\alpha = 1$ control run (black) and with the same profiles divided by three (red) for simulations with SSTs of (a) 300, (b) 299, (c) 297, and (d) 295 K. Dashed curves indicate simulations in which either K_m or K_h is reduced. Black dots indicate 34-kt-wind radii; in (a) the control run’s 34-kt-wind radius is beyond the range depicted.

(Fig. 4a), so the wind speed tendency due to mixing below that level is positive, representing the transport of higher wind speeds downward toward the surface and reducing the vertical shear established by friction. Therefore, when the magnitude of K_m is directly restrained, as in the $K_m/3$ experiment, the wind speed at the 10-m level is impacted, although the influence farther aloft is smaller, increasing the vertical shear. This is another illustration that wind information from a single level may be deceptive.

An alternative explanation of this result may also be pursued by expressing (3) as

$$\left[\frac{\partial U}{\partial t} \right]_{\text{mix}} = \frac{\partial}{\partial z} \left(K_m \frac{\partial U}{\partial z} \right). \quad (4)$$

At the lowest model level, the vertical gradient appears to involve separate K_m values provided by (1) and

implied by the surface layer parameterization, which under standard assumptions (cf. Stensrud 2007; Kepert 2012) is

$$K_m = \kappa (U_* / \phi_m) Z. \quad (5)$$

These assumptions also lead to the logarithmic wind profile under neutral conditions. Augmenting (1) with α means it no longer approaches (5) as $Z \rightarrow 0$. As a consequence, selecting $\alpha < 1$ artificially increases the vertical gradient of K_m , other factors being equal. This has the effect of strengthening the frictional drag and, thus, enhancing the wind shear near the lower boundary.

Whatever the explanation, it is clear that though the vertical shear clearly varies inversely with α , the normalized wind profiles from the GFS $\alpha < 1$ experiments remain logarithmic near the surface (Fig. 12). Also shown are the $K_m/3$ and $K_h/3$ (orange dotted and dashed,

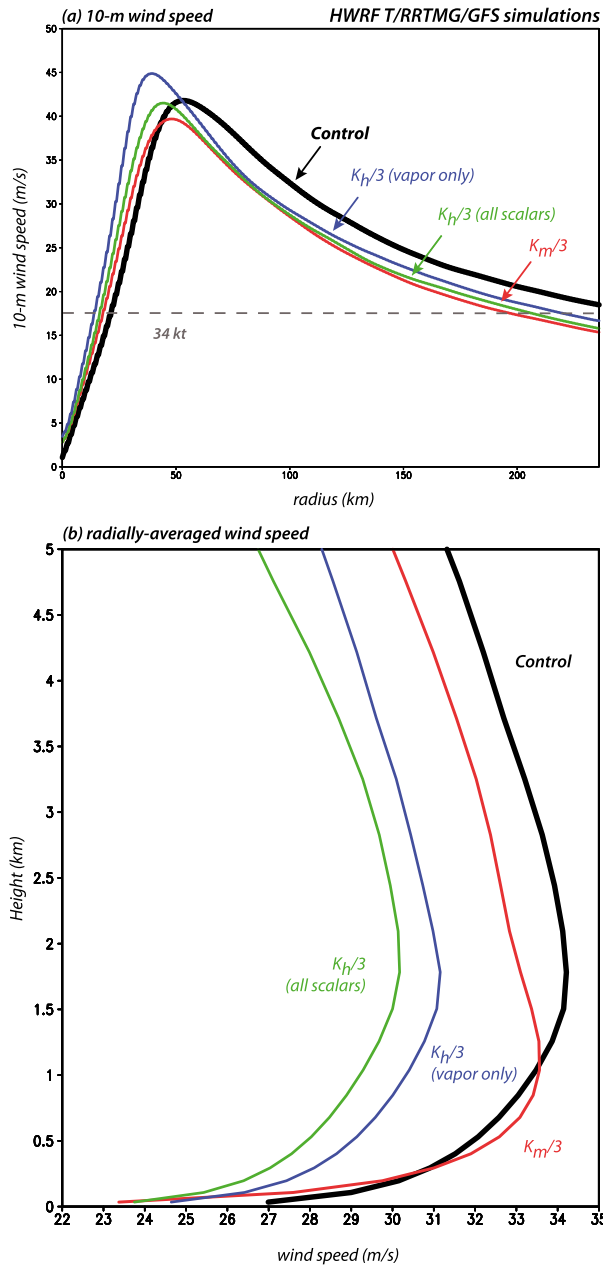


FIG. 10. (a) Temporally and azimuthally averaged 10-m wind speeds (m s^{-1}) from HWRf T/RRTMG/GFS simulations using $\alpha = 1$ with vertical eddy diffusivity unmodified (control; black), reduced momentum mixing ($K_M/3$; red), and reduced scalar mixing ($K_H/3$) applied either to all applicable scalars (green) or just to water vapor (blue). (b) Vertical profiles of wind speed (m s^{-1}) averaged in time and through an annulus extending from 100 to 250 km from the storm center for cases as in (a).

respectively) cases as well as runs made using the YSU (black; see also section 3c), MYJ (gray dotted), and quasi-normal scale elimination (QNSE; Sukoriansky et al. 2006) (gray dashed) PBL schemes. Note that the shear in the $\alpha = 1$ storm is larger than that produced by

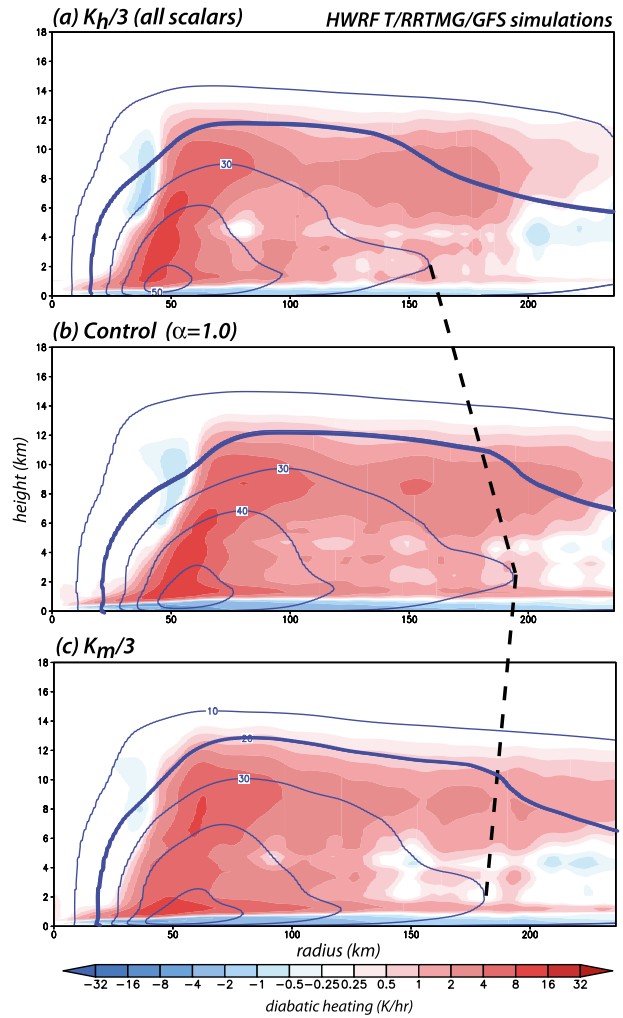


FIG. 11. Microphysics diabatic heating and tangential winds as in Fig. 3, but for HWRf T/RRTMG/GFS $\alpha = 1$ runs using (a) $K_H/3$ (applied to all scalars), (b) unmodified eddy mixing (control), and (c) $K_M/3$. See also Fig. 10.

QNSE and YSU but comparable to the MYJ case and that manipulating K_h independently of K_m has little impact on the shear, which was also suggested by Fig. 10b. The important point is that while the α parameter modulates the mixing of both momentum and scalars, it is the moisture diffusion within the mixed layer that most strongly modulates storm size through the troposphere in our experiment.

Since modifying the mixing applied to some fields can alter the entire circulation, the diffusion not being directly manipulated is also affected to some degree. As a consequence, we also consider a version of the last subsection's fixed- K CM1 experiment in which K_m and K_h are still externally imposed but now manipulated separately, again by reducing the coefficients by two-thirds (also shown on Fig. 9, as dashed curves). We again

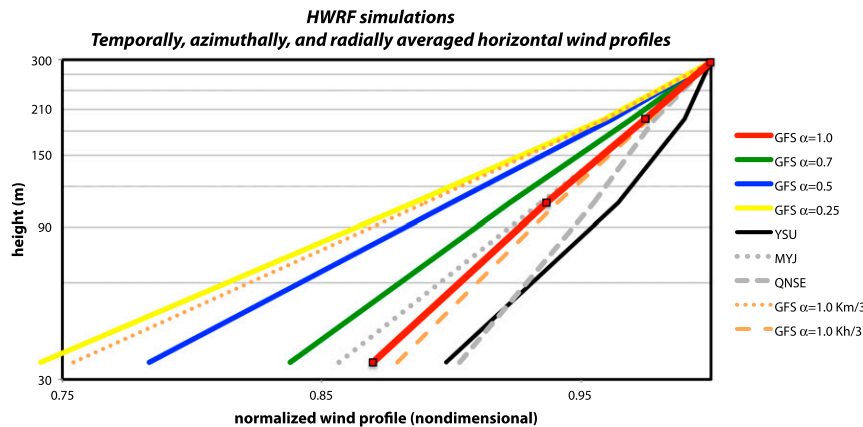


FIG. 12. Vertical profiles of the horizontal wind, averaged in time and through an annulus extending from 100 to 250 km from the storm center, and normalized with respect to the wind speed at about 300 m MSL, from GFS runs with $\alpha = 1, 0.75, 0.5,$ and 0.25 ; the $K_m/3$ and $K_h/3$ (all scalars) tests; and simulations with the YSU, MYJ, and QNSE PBL schemes. Black squares on the GFS $\alpha = 1$ profile indicate model levels. The $K_h/3$ (vapor only) case is indistinguishable from the $K_m/3$ (all scalars) profile shown.

find that K_m has little influence on the storm size as determined from the 10-m-wind profile, while reducing K_h results in narrower storms with smaller eyes, with the differences being more substantial in more favorable environments. The storms with reduced scalar mixing are also stronger than their reduced momentum mixing counterparts, with the apparent exception of the SST = 300-K case. That particular model storm develops an eyewall replacement cycle during the averaging period (not shown), leading to a lower mean intensity.

c. Comparison with YSU scheme

Since its inception, HWRF has used some version of the GFS PBL scheme, while the YSU parameterization is a popular choice with the Advanced Research version of WRF (ARW) core. As these nonlocal schemes evolved from a common ancestor, they unsurprisingly retain many similarities, including the same prescribed parabolic shape function for eddy mixing below the boundary layer depth h . In our tests, however, YSU tends to produce shallower boundary layers that, owing to (1), make the eddy mixing magnitudes smaller and shift the level of maximum mixing closer to the surface (solid black curve on Fig. 4b). One can now anticipate this has an impact on vertical moisture transport and, thus, storm radial extent. At 10-m MSL, the YSU storm's R_{34} is about 182 km, comparable to the GFS simulation with $\alpha = 0.4$ (Fig. 5c).

There are several potentially influential differences between the current YSU and GFS implementations, including their handling of the turbulent Prandtl number (as noted earlier) and the free atmosphere above the PBL, as well as the present need to employ different

surface-layer parameterizations. However, in the present study, by far the most important factor involves the specification of the critical bulk-Richardson number, Rib_{cr} , which influences the PBL height h , with larger Rib_{cr} resulting in greater boundary layer depths. In the original MRF scheme (Hong and Pan 1996), the Rib_{cr} value of 0.5 suggested by Troen and Mahrt (1986) was adopted, while recent practice with the GFS scheme in HWRF has been to set $Rib_{cr} = 0.25$ over water, with optional modification based on the surface Rossby number (cf. Vickers and Mahrt 2004). Although originally set to 0.5 (Hong et al. 2004), YSU evolved to employ different Rib_{cr} values for unstable and stable conditions, and currently uses $Rib_{cr} = 0.0$ for the unstable PBL (Hong 2010).

YSU's stability-dependent handling of Rib_{cr} results in the relatively shallow boundary layer depth seen in Fig. 4b. When the default YSU scheme is altered to adopt an Rib_{cr} of 0.25, as in the current GFS parameterization, the fields and storm structures more closely resemble the GFS results seen earlier (Figs. 4b and 5c). There is more substantial mixing over a greater depth (cf. Figs. 13a,b), producing a larger vertical transport of water vapor above about 700 m MSL (Fig. 13c).³ Averaged through the 30–200-km annulus, the modified YSU mixing (dashed black curve on Fig. 4b) closely resembles that produced by the GFS scheme when $\alpha = 0.7$. The

³ This comparison involves K_h as the YSU scheme permits Pr to become smaller than unity, resulting in larger mixing being applied to scalars than to momentum.

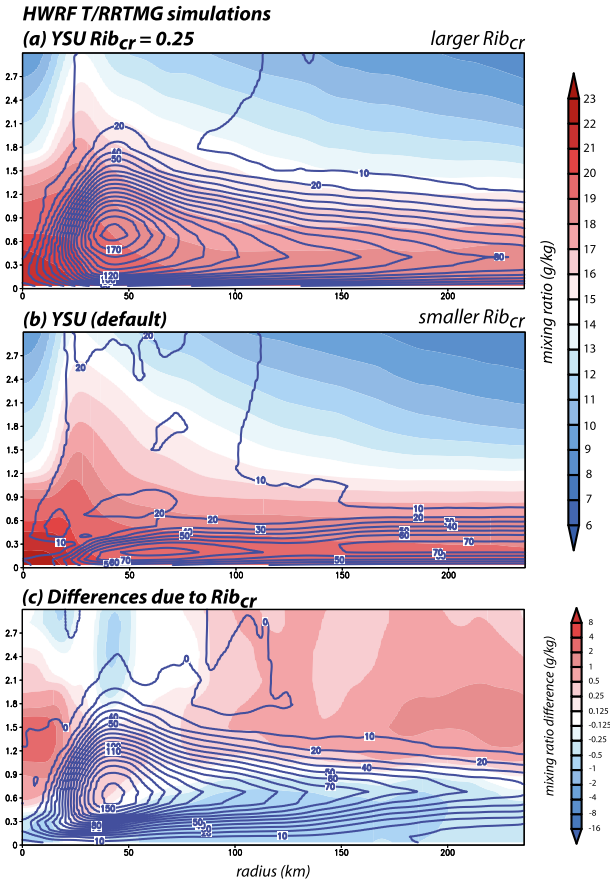


FIG. 13. Water vapor and scalar mixing fields similar to Fig. 6, but for T/RRTMG simulations using YSU with (a) $Rib_{cr} = 0.25$ and (b) the default setup. (c) Difference fields.

wind field at 10-m MSL is also expanded somewhat (Fig. 5c) and comparable to GFS with $\alpha = 0.7$.

As the GFS and YSU parameterizations possess other differences that can impact the hurricane circulation, we consider yet another fixed- K experiment in which the effect of mixing depth is explored (Fig. 14) in a more controlled fashion. For this experiment, the GFS-supplied K_m and K_h fields are either jointly or separately contracted vertically by 50%, mimicking the PBL depths YSU produces in HWRf, but without change in magnitude. Relative to the control configuration (solid black curve), halving the depth of both eddy mixing fields (solid red curve) results in a storm that is narrower in every respect as well as stronger in intensity. As anticipated from prior results, this radial contraction is associated with reduced convective activity in the outer region (not shown). The intensification and width reduction is a consequence of the alteration of the scalar mixing alone (dashed red curve), as halving the depth of just K_m actually results in a small increase of storm width, other factors being equal.

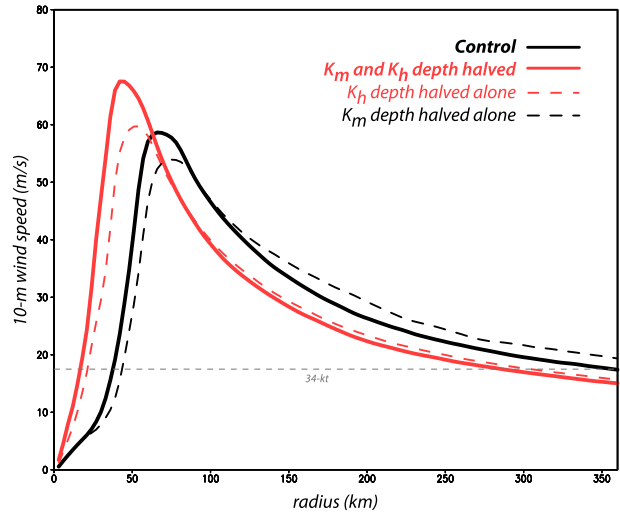


FIG. 14. Temporally averaged 10-m winds similar to Fig. 9, but for CM1 simulations using HWRf-derived vertical eddy mixing profiles with vertical extents that have been unmodified (control; solid black), halved for both K_m and K_h (solid red), halved for K_m only (dashed black), and halved for K_h only (dashed red). The 34-kt-wind threshold is indicated (dashed grey).

Up to this point, we have focused on azimuthally averaged fields, partly for simplicity. However, this disguises the differences among the storms with respect to asymmetric structures, especially beyond the TC inner core. Figure 15 presents mass-weighted mean vertical velocity between the surface and 500 hPa from the HWRf simulations, again temporally averaged over the simulations' final diurnal cycle. The YSU storm (Fig. 15a) is compact, with a narrow and asymmetric eye, and relatively little outer-rainband activity. Raising Rib_{cr} to 0.25 (Fig. 15b) results in an enhanced primary rainband structure (cf. Houze 2010), more closely resembling what the GFS scheme produces with $\alpha = 0.4$ (Fig. 15c). This feature is most prominent when the GFS eddy mixing is even less constrained (Fig. 15d). As these are semi-idealized experiments, there is no correct answer, but it remains that PBL mixing is clearly influential in modulating outer-storm structure.

d. Comparison with selected axisymmetric studies

In contrast to our study, the axisymmetric studies of Bryan and Rotunno (2009), Bryan (2012), Chavas and Emanuel (2014), and Frisius (2015) reported little sensitivity of TC size to vertical mixing, which can be manipulated via the vertical mixing length l_v . Bryan (2012) found "a slight tendency for smaller R_{34} as l_v decreases," and variations of 20–28 km are seen for that paper's two setups when his recommended values for horizontal mixing length ($l_h = 1000$ m) and the enthalpy-drag coefficient ratio ($C_k/C_d = 0.5$) were adopted (see his

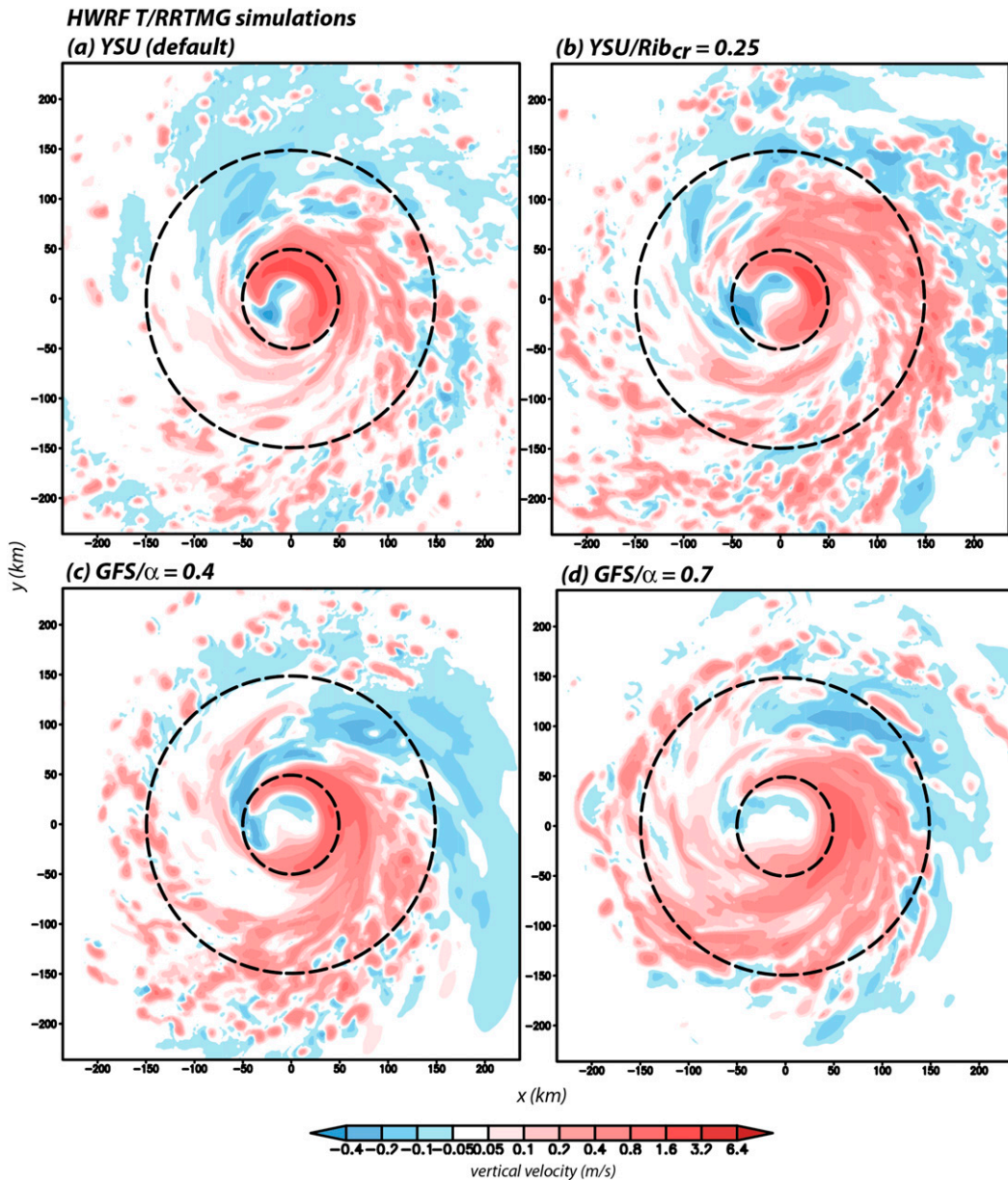


FIG. 15. Mass-weighted mean vertical velocity (m s^{-1}) from HWRF T/RRTMG simulations using (a) the default YSU scheme with $\text{Rib}_{\text{cr}} = 0.0$, (b) the YSU scheme with $\text{Rib}_{\text{cr}} = 0.25$, (c) the GFS scheme with (c) $\alpha = 0.4$, and (d) the GFS scheme with $\alpha = 0.7$. Range rings of 50 and 150 km are depicted, and tops of plots represent north.

Fig. 7). Frisius (2015) suggested that the lifetime of a TC is too short for vertical mixing sensitivity to be relevant. However, there are a number of potentially important differences between their experiments and ours, the most influential one being the treatment of atmospheric radiation.

In this subsection, we employ axisymmetric CM1 simulations configured similarly to Bryan and Rotunno (2009), albeit with somewhat coarser (3 km) radial grid spacing and Thompson microphysics. Vertical mixing lengths of 100 and 25 m are examined with l_h fixed at

1000 m. The cited axisymmetric studies employed somewhat different, and yet all highly simplified, radiation treatments in lieu of a full parameterization, so we adopt the approach employed by Bryan and Rotunno (2009) in which a sponge term mimicking clear-sky cooling is added to the temperature equation. This approach, which naturally lacks a diurnal cycle and ignores CRF, is identified as “R-E relaxation” after Rotunno and Emanuel (1987). As in Bryan and Rotunno (2009), cooling is capped at 2 K day^{-1} . The C_k/C_d ratio varies

with wind speed but remains in the range from 0.5 to 0.7 between the RMW and R_{34} .

Owing to friction, a storm's fastest winds are typically located hundreds of meters above the surface, and both R-E relaxation cases attain temporally averaged peak tangential velocities [computed in the manner of Bryan and Rotunno (2009)] of about 90 m s^{-1} (not shown), consistent with the values provided in Fig. 2 of Bryan and Rotunno (2009). At 10 m MSL, however, both are quite compact relative to the HWRF simulations examined previously, with R_{34} of only about 65 km (blue curves in Fig. 16a). The narrowness persists through the 12-day simulation period following maturity (Fig. 17a) and extends through the troposphere, associated with a very clear absence of outer-convective activity (shown for $l_v = 100 \text{ m}$ in Fig. 18a). The vertical eddy mixing field (shown for $l_v = 100 \text{ m}$ in Fig. 19b) and applied equally to momentum and scalars bears some resemblance to the HWRF runs using GFS (Fig. 6a) in that both have a parabolic vertical shape with a maximum at about 0.5–0.6 km MSL beyond the RMW. While fairly large values of mixing extend vertically into the eyewall, a characteristic explained by Kepert (2012), note the mixing strength tapers off much more rapidly in the radial direction.

In contrast, the CM1 simulations employing Goddard radiation (with CRF active) yield much wider storms (black curves in Fig. 16a), which are more comparable to the HWRF simulations and expand progressively with time (Fig. 17b). These results are consistent with the findings of Hakim (2011). There is a suggestion of more outer convective activity (shown for $l_v = 100 \text{ m}$ in Fig. 18b) and greater sensitivity to the vertical mixing length (Figs. 16a and 17b). In line with the broader and stronger storm circulation, the vertical eddy mixing field is larger in both magnitude and radial extent (Fig. 19a). As anticipated from prior results, the more vigorous mixing contributes to increasing the water vapor content in the upper portion of the boundary layer relative to the R-E case (Fig. 19c).

The three principal differences between the R-E relaxation and Goddard/CRF runs for a given l_v setting are the manner in which clear-sky radiative cooling is computed, inclusion or exclusion of cloud-radiative feedback, and the amount of the boundary layer eddy mixing. Our analysis suggests all three factors contribute to making the Goddard/CRF storm wider, with eddy mixing being the least important. First, the effect of the handling of clear-sky atmospheric radiation alone is tested using Goddard radiation but with CRF deactivated. Relative to the R-E simulation, the CRF-off storm is both stronger and wider (black curve in Fig. 16b; Fig. 18c), although still narrower than its CRF-active counterpart and with a much slower rate of radial

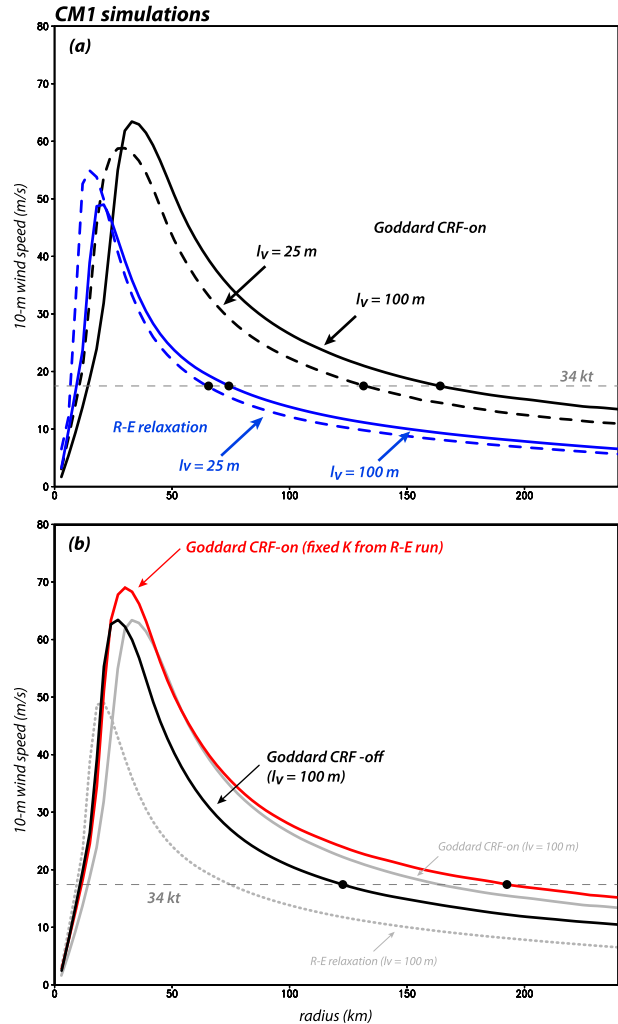


FIG. 16. The 10-m wind speed from CM1 simulations, averaged between days 8 and 12. (a) Simulations using R-E relaxation (blue curves) and Goddard radiation with CRF on (black curves) with $l_v = 100$ (solid) and 50 m (dashed). (b) Simulations using Goddard radiation with CRF off and $l_v = 100 \text{ m}$ (black curve) and a fixed- K run using the R-E ($l_v = 100 \text{ m}$) simulation's eddy mixing field (red curve). The $l_v = 100\text{-m}$ profiles from (a) are included in gray for reference.

expansion. Even with transparent clouds, however, organization is more rapid and greater sensitivity to l_v is apparent (Fig. 17c).

Second, the effect of eddy mixing in isolation can be tested via a final fixed- K experiment, this time utilizing the R-E case's temporally averaged $K_m (=K_h)$ field (Fig. 19b). Again, this is externally applied from the start of the simulation, and Goddard radiation is employed with CRF active. Despite the relatively weak and restricted mixing at outer radii, the storm is still able to organize rapidly (Fig. 17d), develop radially extensive convective activity (Fig. 18d), and attain a 10-m-wind

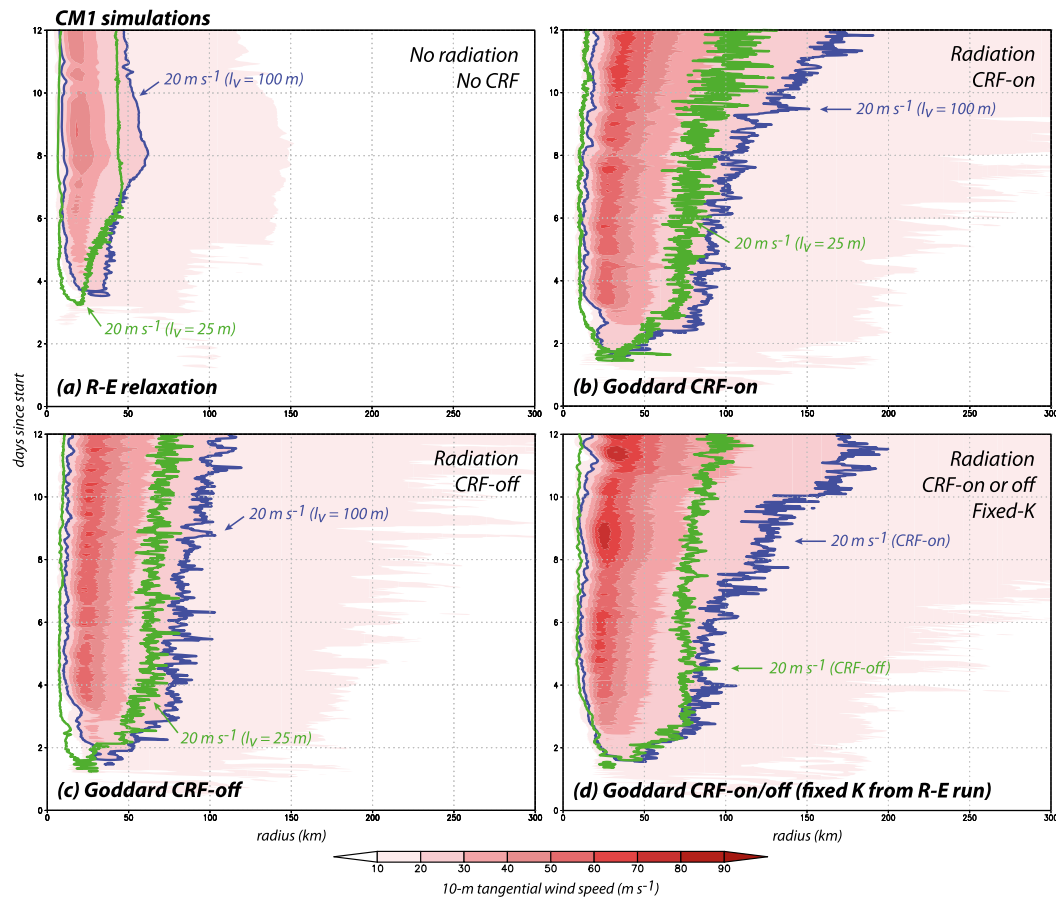


FIG. 17. Hovmöller (time vs radius) diagrams of tangential wind speed at 10 m MSL, with 20 m s^{-1} contour bolded, for CM1 simulations with $l_v = 100$ m and using (a) R-E relaxation, (b) Goddard radiation with CRF on, (c) Goddard radiation with CRF off, and (d) Goddard with CRF on, but with fixed eddy mixing from the R-E simulation in (a). In (a) and (b), 20 m s^{-1} contours from corresponding simulations using $l_v = 25$ m are shown in green. In (d), 20 m s^{-1} contours for CRF-off version shown in green.

profile comparable to the standard CRF example (red curve in Fig. 16b). That this is mostly due to CRF is demonstrated by the much slower expansion of this experiment's CRF-off version (20 m s^{-1} contour superposed in green in Fig. 17d), which more closely resembles the other CRF-off storm (Fig. 17c) with respect to size and expansion rate. In agreement with our previous fixed- K experiments, these results suggest that a vertical mixing field that evolves with time to become radially extensive can assist in the progressive expansion of a tropical cyclone but is not absolutely necessary, particularly when clouds are permitted to interact with radiation.

4. Discussion and summary

Bu et al. (2014) demonstrated that cloud-radiative forcing (CRF) can exert a substantial influence on

numerically simulated tropical cyclones (TCs), especially with respect to the storm's horizontal scale. Specifically, it is the within-cloud longwave warming component of CRF that indirectly enhances convective activity in the TC outer core, thereby generating the diabatic heating that broadens the wind field. They further established that the radiation scheme employed by the operational HWRF, which derived from the old GFDL parameterization, was very deficient in handling CRF, to the point that it was essentially absent. However, as mentioned in the introduction, when HWRF was applied to historical cases using a more realistic radiation package, model skill with respect to important storm characteristics, such as intensity, position, and size, was degraded. In particular, most storms developed a positive size bias with respect to R_{34} , the radius of the 34-kt (17.5 m s^{-1}) wind at 10 m above the surface, one of the important metrics used in model verification.

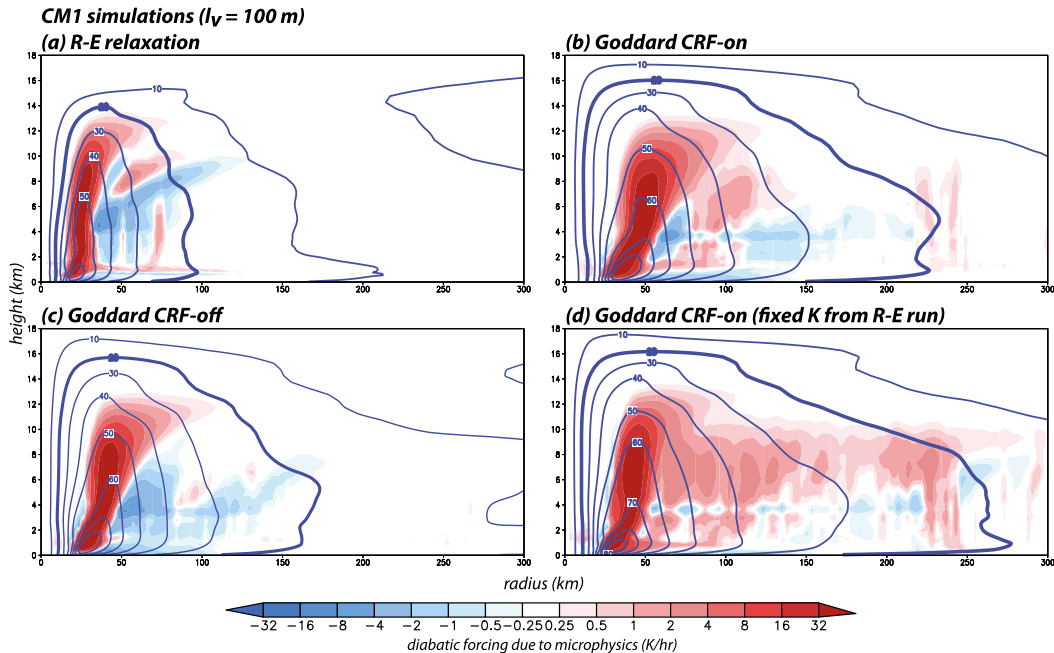


FIG. 18. Radius vs height cross sections showing the temporally averaged microphysics diabatic forcing (shaded) and tangential wind (m s^{-1}) from CM1 simulations using (a) R-E relaxation, (b) Goddard radiation with CRF on, (c) Goddard radiation with CRF off, and (d) Goddard with CRF on, but with fixed eddy mixing from the R-E simulation in (a). The 20 m s^{-1} contours are bolded. All simulations used $l_v = 100$ m and were averaged between days 8 and 12.

That result motivated a study of how and why the planetary boundary layer (PBL) and its parameterization affect storm size, in cooperation and competition with CRF. Our principal finding is that vertical mixing of scalars in the boundary layer, primarily water vapor, also influences storm size via modulating outer-core convective activity. In this case, it is eddy mixing that helps transport water vapor to the top of the boundary layer, elevating the relative humidity there, and making the outer core more favorable for convection. Thus, a compelling parallel is seen with respect to CRF, the difference being that the heating associated with in-cloud warming was focused above the boundary layer, while the PBL influence is essentially “bottom up” from the sea surface.

As a consequence, we see why TC structure is sensitive to the PBL parameterization, particularly with respect to the magnitude and shape of the eddy diffusion distributions they generate. This was demonstrated using HWRF’s operational boundary layer code, the GFS PBL scheme, which was modified in the past to incorporate a tuning parameter α to throttle mixing in the TC inner core (Gopalakrishnan et al. 2013) because observations (e.g., Zhang et al. 2011a) suggested the model was too diffusive. We showed that α has a profound influence on R_{34} . Indeed, we believe that it was

the excessive diffusion produced by the GFS scheme that was previously compensating for the lack of cloud-radiative forcing in HWRF such that when the radiation issue was fixed, the simulated TCs developed a positive size bias, leading to poorer wind structure, intensity, and position forecasts.

Eddy mixing applied to momentum also appears to influence storm size, at least relatively close to the surface. However, what changed the most was the vertical shear, as the winds farther aloft were less impacted. Since the breadth of the 10-m-MSL wind field is one of the parameters used to judge model forecast skill, and information from farther aloft is often absent, this result raises the possibility that available storm size and/or intensity information can be skewed or misinterpreted. That said, examination of retrospective cases made using HWRF suggested that TCs are not always responsive to variations in the eddy mixing and the sensitivity is diminished when the TC environment is generally less favorable, which we demonstrated via experiments in which the sea surface temperature (SST) was lowered.

The GFS and YSU PBL schemes share a common ancestor and represent parameterizations that determine PBL height based on near-surface vertical stability and wind shear (cf. Vickers and Mahrt 2004). We

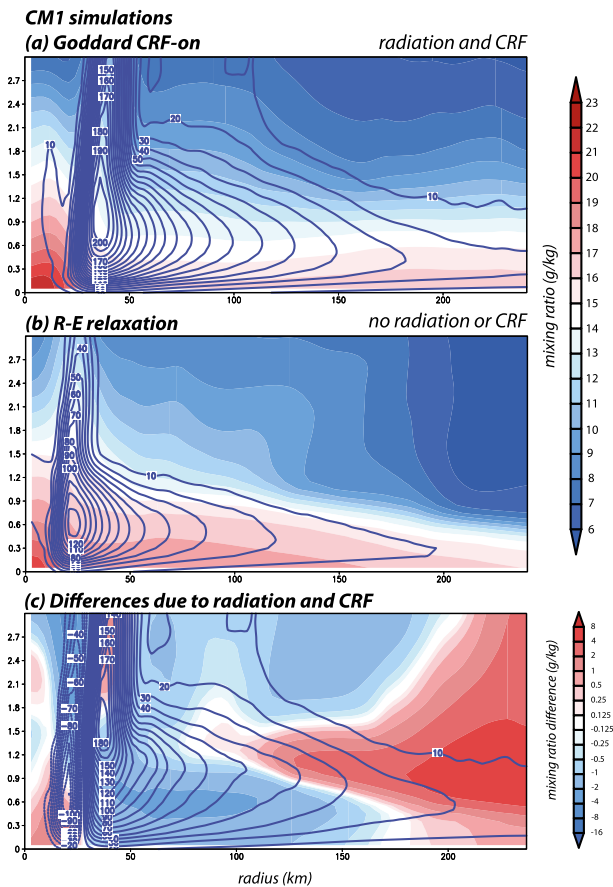


FIG. 19. As in Fig. 6, but for CM1 simulations using (a) Goddard with CRF on and (b) R-E relaxation. (c) The difference fields. Both simulations used $l_v = 100$ m and were averaged between days 8 and 12.

demonstrated that how the critical Richardson number, Ri_{cr} , was specified in these schemes had a major impact on the magnitude and depth of the eddy mixing, indirectly influencing TC size through vertical diffusion of boundary layer scalars. This finding motivates closer study in the future as it appears to provide a more physically defensible way of modulating mixing, especially because there is uncertainty with respect to the structure of the hurricane inner core and how the PBL depth should be defined (cf. Zhang et al. 2011b). Finally, through a comparison with recent axisymmetric studies, we appreciate that vertical mixing can indeed influence the progressive expansion of a TC in this restricted physical framework, but it does so most efficiently when acting with the assistance of cloud-radiative forcing.

Acknowledgments. The authors gratefully acknowledge the assistance of Drs. Ligia Bernardet, Mrinal Biswas, Gregory Thompson, Christina Holt, and three anonymous reviewers. This work was supported by the

National Atmospheric and Oceanic Administration's Hurricane Forecast Improvement Program (HFIP) under Grant NA12NWS4680009, by the National Aeronautics and Space Administration's Hurricane Science Research Program under Grant NNX12AJ83G, and by the Developmental Testbed Center (DTC) visitor program. The DTC Visitor Program is funded by the National Oceanic and Atmospheric Administration, the National Center for Atmospheric Research, and the National Science Foundation.

REFERENCES

- Bender, M., 1997: The effect of relative flow on the asymmetric structure in the interior of hurricanes. *J. Atmos. Sci.*, **54**, 703–724, doi:10.1175/1520-0469(1997)054<0703:TEORFO>2.0.CO;2.
- Bernardet, L., S. Bao, R. Yablonsky, D. Stark, and T. Brown, 2013: Community HWRP users guide V3.5A. NOAA Tech. Memo. OAR GSD-43, 140 pp. [Available online at http://www.dtcenter.org/HurrWRF/users/docs/users_guide/HWRP_v3.5a_Users_Guide.pdf.]
- Braun, S. A., and W.-K. Tao, 2000: Sensitivity of high-resolution simulations of Hurricane Bob (1991) to planetary boundary layer parameterizations. *Mon. Wea. Rev.*, **128**, 3941–3961, doi:10.1175/1520-0493(2000)129<3941:SOHRSO>2.0.CO;2.
- Bryan, G. H., 2012: Effects of surface exchange coefficients and turbulence length scales on the intensity and structure of numerically simulated hurricanes. *Mon. Wea. Rev.*, **140**, 1125–1143, doi:10.1175/MWR-D-11-00231.1.
- , and R. Rotunno, 2009: The maximum intensity of tropical cyclones in axisymmetric numerical model simulations. *Mon. Wea. Rev.*, **137**, 1770–1789, doi:10.1175/2008MWR2709.1.
- Bu, Y. P., and R. G. Fovell, 2015: Model physics influences on tropical cyclone size. *16th Conf. on Mesoscale Processes*, Boston, MA, Amer. Meteor. Soc., 17.2. [Available online at <https://ams.confex.com/ams/16Meso/webprogram/Paper274629.html>.]
- , —, and K. L. Corbosiero, 2014: Influence of cloud-radiative forcing on tropical cyclone structure. *J. Atmos. Sci.*, **71**, 1644–1662, doi:10.1175/JAS-D-13-0265.1.
- Cao, Y., R. G. Fovell, and K. L. Corbosiero, 2011: Tropical cyclone track and structure sensitivity to initialization in idealized simulations: A preliminary study. *Terr. Atmos. Oceanic Sci. J.*, **22**, 559–578, doi:10.3319/TAO.2011.05.12.01(TM).
- Carrasco, C. A., C. W. Landsea, and Y.-L. Lin, 2014: The influence of tropical cyclone size on its intensification. *Wea. Forecasting*, **29**, 582–590, doi:10.1175/WAF-D-13-00092.1.
- Chavas, D. R., and K. Emanuel, 2014: Equilibrium tropical cyclone size in an idealized state of axisymmetric radiative-convective equilibrium. *J. Atmos. Sci.*, **71**, 1663–1680, doi:10.1175/JAS-D-13-0155.1.
- , N. Lin, and K. Emanuel, 2015: A model for the complete radial structure of the tropical cyclone wind field. Part I: Comparison with observed structure. *J. Atmos. Sci.*, **72**, 3647–3662, doi:10.1175/JAS-D-15-0014.1.
- , —, W. Dong, and Y. Lin, 2016: Observed tropical cyclone size revisited. *J. Climate*, **29**, 2923–2939, doi:10.1175/JCLI-D-15-0731.1.
- Chou, M.-D., and M. J. Suarez, 1994: An efficient thermal infrared radiation parameterization for use in general circulation models. NASA Tech. Memo. 104606, 85 pp. [Available online at <http://citeseerx.ist.psu.edu/viewdoc/download?doi=10.1.1.26.4850&rep=rep1&type=pdf>.]

- DeMaria, M., R. T. DeMaria, J. A. Knaff, and D. Molenaar, 2012: Tropical cyclone lightning and rapid intensity change. *Mon. Wea. Rev.*, **140**, 1828–1842, doi:10.1175/MWR-D-11-00236.1.
- Emanuel, K. A., 1986: An air-sea interaction theory for tropical cyclones. Part I: Steady-state maintenance. *J. Atmos. Sci.*, **43**, 585–605, doi:10.1175/1520-0469(1986)043<0585:AASITF>2.0.CO;2.
- Fiorino, M. J., and R. L. Elsberry, 1989: Some aspects of vortex structure related to tropical cyclone motion. *J. Atmos. Sci.*, **46**, 975–990, doi:10.1175/1520-0469(1989)046<0975:SAOVS>2.0.CO;2.
- Fovell, R. G., and H. Su, 2007: Impact of cloud microphysics on hurricane track forecasts. *Geophys. Res. Lett.*, **34**, L24810, doi:10.1029/2007GL031723.
- , K. L. Corbosiero, A. Seifert, and K. N. Liou, 2010: Impact of cloud-radiative processes on hurricane track. *Geophys. Res. Lett.*, **37**, L07808, doi:10.1029/2010GL042691.
- , Y. P. Bu, K. L. Corbosiero, W.-W. Tung, Y. Cao, H.-C. Kuo, L.-H. Hsu, and H. Su, 2016: Influence of cloud microphysics and radiation on tropical cyclone structure and motion. *Multiscale Convection-Coupled Systems in the Tropics: A Tribute to Dr. Michio Yanai, Meteor. Monogr.*, No. 56, Amer. Meteor. Soc., 11.1–11.27, doi:10.1175/AMSMONOGRAPHIS-D-15-0006.1.
- Frisius, T., 2015: What controls the size of a tropical cyclone? Investigations with an axisymmetric model. *Quart. J. Roy. Meteor. Soc.*, **141**, 2457–2470, doi:10.1002/qj.2537.
- Gopalakrishnan, S. G., F. Marks, J. A. Zhang, X. Zhang, J.-W. Bao, and V. Tallapragada, 2013: A study of the impacts of vertical diffusion on the structure and intensity of the tropical cyclones using the high-resolution HWRf system. *J. Atmos. Sci.*, **70**, 524–541, doi:10.1175/JAS-D-11-0340.1.
- Hakim, G. J., 2011: The mean state of axisymmetric hurricanes in statistical equilibrium. *J. Atmos. Sci.*, **68**, 1364–1376, doi:10.1175/2010JAS3644.1.
- Hill, K. A., and G. M. Lackmann, 2009: Analysis of idealized tropical cyclone simulations using the Weather Research and Forecasting Model: Sensitivity to turbulence parameterization and grid spacing. *Mon. Wea. Rev.*, **137**, 745–765, doi:10.1175/2008MWR2220.1.
- Holland, G. J., 1997: The maximum potential intensity of tropical cyclones. *J. Atmos. Sci.*, **54**, 2519–2541, doi:10.1175/1520-0469(1997)054<2519:TMPIOT>2.0.CO;2.
- Holt, C., L. Bernardet, T. Brown, and R. Yablonsky, 2014: Community HWRf users' guide V3.6a. Developmental Testbed Center Tech. Rep., 128 pp. [Available online at http://www.dtcenter.org/HurrWRF/users/docs/users_guide/HWRf_UG_v3.6a.pdf.]
- Hong, S.-Y., 2010: A new stable boundary-layer mixing scheme and its impact on the simulated East Asian summer monsoon. *Quart. J. Roy. Meteor. Soc.*, **136**, 1481–1496, doi:10.1002/qj.665.
- , and H.-L. Pan, 1996: Nonlocal boundary layer vertical diffusion in a medium-range forecast model. *Mon. Wea. Rev.*, **124**, 2322–2339, doi:10.1175/1520-0493(1996)124<2322:NBLVDI>2.0.CO;2.
- , J. Dudhia, and S.-H. Chen, 2004: A revised approach to ice microphysical processes for the bulk parameterization of clouds and precipitation. *Mon. Wea. Rev.*, **132**, 103–120, doi:10.1175/1520-0493(2004)132<0103:ARATIM>2.0.CO;2.
- , Y. Noh, and J. Dudhia, 2006: A new vertical diffusion package with an explicit treatment of entrainment processes. *Mon. Wea. Rev.*, **134**, 2318–2341, doi:10.1175/MWR3199.1.
- Houze, R. A., 2010: Clouds in tropical cyclones. *Mon. Wea. Rev.*, **138**, 293–344, doi:10.1175/2009MWR2989.1.
- Iacono, M. J., J. S. Delamere, E. J. Mlawer, M. W. Shephard, S. A. Clough, and W. D. Collins, 2008: Radiative forcing by long-lived greenhouse gases: Calculations with the AER radiative transfer models. *J. Geophys. Res.*, **113**, D13103, doi:10.1029/2008JD009944.
- Janjić, Z. I., 1990: The step-mountain coordinate: Physical package. *Mon. Wea. Rev.*, **118**, 1429–1443, doi:10.1175/1520-0493(1990)118<1429:TSMCPP>2.0.CO;2.
- Jordan, C. L., 1958: Mean soundings for the West Indies area. *J. Meteor.*, **15**, 91–97, doi:10.1175/1520-0469(1958)015<0091:MSFTWI>2.0.CO;2.
- Keper, J. D., 2012: Choosing a boundary layer parameterization for tropical cyclone modeling. *Mon. Wea. Rev.*, **140**, 1427–1445, doi:10.1175/MWR-D-11-00217.1.
- Kimball, S. K., and M. S. Mulekar, 2004: A 15-year climatology of North Atlantic tropical cyclones. Part I: Size parameters. *J. Climate*, **17**, 3555–3576, doi:10.1175/1520-0442(2004)017<3555:AYCONA>2.0.CO;2.
- Knaff, J. A., C. J. Slocum, K. D. Musgrave, C. R. Sampson, and B. R. Strahl, 2016: Using routinely available information to estimate tropical cyclone wind structure. *Mon. Wea. Rev.*, **144**, 1233–1247, doi:10.1175/MWR-D-15-0267.1.
- Lin, N., and D. Chavas, 2012: On hurricane parametric wind and applications in storm surge modeling. *J. Geophys. Res.*, **117**, D09120, doi:10.1029/2011JD017126.
- Lin, Y., M. Zhao, and M. Zhang, 2015: Tropical cyclone rainfall area controlled by relative sea surface temperature. *Nat. Commun.*, **6**, 6591, doi:10.1038/ncomms7591.
- Mallen, K. J., M. T. Montgomery, and B. Wang, 2005: Reexamining the near-core radial structure of the tropical cyclone primary circulation: Implications for vortex resiliency. *J. Atmos. Sci.*, **62**, 408–425, doi:10.1175/JAS-3377.1.
- May, P. T., and G. J. Holland, 1999: The role of potential vorticity generation in tropical cyclone rainbands. *J. Atmos. Sci.*, **56**, 1224–1228, doi:10.1175/1520-0469(1999)056<1224:TROPVG>2.0.CO;2.
- Nolan, D. S., J. A. Zhang, and D. P. Stern, 2009a: Evaluation of planetary boundary layer parameterizations in tropical cyclones by comparison of in situ observations and high-resolution simulations of Hurricane Isabel (2003). Part I: Initialization, maximum winds, and the outer-core boundary layer. *Mon. Wea. Rev.*, **137**, 3651–3674, doi:10.1175/2009MWR2785.1.
- , D. P. Stern, and J. A. Zhang, 2009b: Evaluation of planetary boundary layer parameterizations in tropical cyclones by comparison of in situ observations and high-resolution simulations of Hurricane Isabel (2003). Part II: Inner-core boundary layer and eyewall structure. *Mon. Wea. Rev.*, **137**, 3675–3698, doi:10.1175/2009MWR2786.1.
- Ooyama, K., 1969: Numerical simulation of the life cycle of tropical cyclones. *J. Atmos. Sci.*, **26**, 3–40, doi:10.1175/1520-0469(1969)026<0003:NSOTLC>2.0.CO;2.
- Rotunno, R., and K. A. Emanuel, 1987: An air-sea interaction theory for tropical cyclones. Part II: Evolutionary study using a nonhydrostatic axisymmetric numerical model. *J. Atmos. Sci.*, **44**, 542–561, doi:10.1175/1520-0469(1987)044<0542:AAITFT>2.0.CO;2.
- Smith, R. K., 1968: The surface boundary layer of a hurricane. *Tellus*, **20**, 473–484, doi:10.1111/j.2153-3490.1968.tb00388.x.
- , and G. L. Thomsen, 2010: Dependence of tropical-cyclone intensification on the boundary-layer representation in a numerical model. *Quart. J. Roy. Meteor. Soc.*, **136**, 1671–1685, doi:10.1002/qj.687.
- Stensrud, D. J., 2007: *Parameterization Schemes: Keys to Understanding Numerical Weather Prediction Models*. Cambridge University Press, 488 pp.

- Sukoriansky, S., B. Galperin, and V. Perov, 2006: A quasi-normal scale elimination model of turbulence and its application to stably stratified flows. *Nonlinear Processes Geophys.*, **13**, 9–22, doi:10.5194/npg-13-9-2006.
- Tallapragada, V., and Coauthors, 2014: Hurricane Weather Research and Forecasting (HWRF) model: 2014 scientific documentation. Developmental Testbed Center Tech. Rep. HWRF v3.6a, 105 pp. [Available online at http://www.dtcenter.org/HurrWRF/users/docs/scientific_documents/HWRFv3.6a_ScientificDoc.pdf.]
- , and Coauthors, 2015: Hurricane Weather Research and Forecasting (HWRF) model: 2015 scientific documentation. Developmental Testbed Center Tech. Rep. HWRF v3.7a, 113 pp. [Available online at http://www.dtcenter.org/HurrWRF/users/docs/scientific_documents/HWRF_v3.7a_SD.pdf.]
- Thompson, G., P. R. Field, R. M. Rasmussen, and W. D. Hall, 2008: Explicit forecasts of winter precipitation using an improved bulk microphysics scheme. Part II: Implementation of a new snow parameterization. *Mon. Wea. Rev.*, **136**, 5095–5115, doi:10.1175/2008MWR2387.1.
- Troen, I., and L. Mahrt, 1986: A simple model of the atmospheric boundary layer; sensitivity to surface evaporation. *Boundary Layer Meteor.*, **37**, 129–148, doi:10.1007/BF00122760.
- Van Sang, N., R. K. Smith, and M. T. Montgomery, 2008: Tropical-cyclone intensification and predictability in three dimensions. *Quart. J. Roy. Meteor. Soc.*, **134**, 563–582, doi:10.1002/qj.235.
- Vickers, D., and L. Mahrt, 2004: Evaluating formulations of stable boundary layer height. *J. Appl. Meteor.*, **43**, 1736–1749, doi:10.1175/JAM2160.1.
- Wang, Y., 2009: How do outer spiral rainbands affect tropical cyclone structure and intensity? *J. Atmos. Sci.*, **66**, 1250–1273, doi:10.1175/2008JAS2737.1.
- Wu, L., W. Tian, Q. Liu, J. Cao, and J. A. Knaff, 2015: Implications of the observed relationship between tropical cyclone size and intensity over the western North Pacific. *J. Climate*, **28**, 9501–9506, doi:10.1175/JCLI-D-15-0628.1.
- Zhang, J. A., F. D. Marks, M. T. Montgomery, and S. Lorsolo, 2011a: An estimation of turbulent characteristics in the low-level region of intense hurricanes Allen (1980) and Hugo (1989). *Mon. Wea. Rev.*, **139**, 1447–1462, doi:10.1175/2010MWR3435.1.
- , R. F. Rogers, D. S. Nolan, and F. D. Marks, 2011b: On the characteristic height scales of the hurricane boundary layer. *Mon. Wea. Rev.*, **139**, 2523–2535, doi:10.1175/MWR-D-10-05017.1.